

South Dakota State University
**Open PRAIRIE: Open Public Research Access Institutional
Repository and Information Exchange**


Electronic Theses and Dissertations

2018

Electro-magnetic Responsive Ni_{0.5}Zn_{0.5}Fe₂O₄ Nano-particle Composite

Jaiprakash Kanagaraj
South Dakota State University

Follow this and additional works at: <https://openprairie.sdstate.edu/etd>

 Part of the [Electromagnetics and Photonics Commons](#), [Materials Science and Engineering Commons](#), and the [Nanotechnology Fabrication Commons](#)

Recommended Citation

Kanagaraj, Jaiprakash, "Electro-magnetic Responsive Ni_{0.5}Zn_{0.5}Fe₂O₄ Nano-particle Composite" (2018). *Electronic Theses and Dissertations*. 2428.
<https://openprairie.sdstate.edu/etd/2428>

This Thesis - Open Access is brought to you for free and open access by Open PRAIRIE: Open Public Research Access Institutional Repository and Information Exchange. It has been accepted for inclusion in Electronic Theses and Dissertations by an authorized administrator of Open PRAIRIE: Open Public Research Access Institutional Repository and Information Exchange. For more information, please contact michael.biondo@sdstate.edu.

ELECTRO-MAGNETIC RESPONSIVE $\text{Ni}_{0.5}\text{Zn}_{0.5}\text{Fe}_2\text{O}_4$ NANO-PARTICLE
COMPOSITE

BY

JAIPRAKASH KANAGARAJ

A thesis submitted in fulfillment of the requirements for the

Master of Science

Major in Mechanical Engineering

South Dakota State University

2018

ELECTRO-MAGNETIC RESPONSIVE $\text{Ni}_{0.5}\text{Zn}_{0.5}\text{Fe}_2\text{O}_4$ NANO-PARTICLE
COMPOSITE

This thesis is approved as a creditable and independent investigation by a candidate for the Master of Science in Mechanical Engineering degree and is acceptable for meeting the thesis requirements for this degree. Acceptance of this does not imply that the conclusions reached by the candidates are necessarily the conclusions of the major department.

Dr. Zhong Hu, Ph.D.

Thesis Advisor

Date

Dr. Kurt Bassett, Ph.D.

Head, Department of Mechanical Engineering Date

Dean, Graduate School

Date

ACKNOWLEDGEMENTS

Foremost, I would like to express my sincere gratitude to my advisor Professor Zhong Hu for continuous support of my graduate study, research, and employment with his patience and his knowledge. His encouragement during my research and his willingness to investigate for the true answers and understanding of the research problems has shown me how to work with integrity. From the beginning of the project to the completion Dr. Hu has guided me and assisted me with understanding this subject.

Besides my advisor, I would like to thank Dr. Fan and Dr. Kharel for giving me the chance to work in their labs and using equipment to perform this project.

My sincere thanks go to the graduate school of South Dakota State University for allowing me to perform this research with ANSYS, Inc.

Finally, my special thanks go to my parents for their support. A special thank you to them for being patient with me and encouraging me.

CONTENTS

LIST OF FIGURES	vi
LIST OF TABLES	viii
ABSTRACT	ix
Chapter 1 Introduction	1
1.1 Significance.....	1
1.2 Background.....	1
1.3 Literature Review.....	3
1.4 Motivation.....	9
1.5 Objective.....	10
Chapter 2 FUNDAMENTAL OF EM WAVE ABSORPTION	12
2.1. Maxwell`s Equation	12
2.2. EM Wave Absorption Ability.....	15
2.3. EM Wave Absorption Mechanism.....	16
2.3.1. Magnetic Loss Mechanism	16
2.3.2. Dielectric Loss	18
2.4. Influence Factors for Electromagnetic Wave Absorption	20
2.4.1. Complex Permittivity.....	20
2.4.2. Complex Permeability	21
2.4.3. Electric Conductivity	21
2.4.4. Nano-effect Morphology	22
2.4.5 Structure of Material	23
2.5. Finite Element Analysis (FEA) in ANSYS	23
2.5.1. Dielectric Model	25
2.5.2. Magnetic Model.....	27
2.6. Review of Conventional Analytic Theories for the Properties of a Dielectric composite or a Magnetic Composite.....	28
2.6.1. Maxwell-Garnett (M-G) Theory.....	28
2.6.2. Bruggeman Theory	29
Chapter 3 FEA MODELING CONSTRUCTION	31
3.1. Typical FEA Process.....	31
3.2 Introduction of Electromagnetic Element in ANSYS.....	32
3.3. REV Model Construction	34
3.3.1 REV Distribution Model.....	37
3.3.2 REV Shape Model	38
3.3.3 Monte Carlo model	40
3.4. Material Properties.....	40
3.5. REV Meshing.....	42

3.6.	REV Boundary Condition Setup.....	43
3.6.1.	Permittivity	43
3.6.2.	Permeability	44
Chapter 4 FABRICATION OF NANO-PARTICE REINFORCED EPOXY BASED COMPOSITES.....		47
4.1.	General Description of Fabrication Experiment Design.....	47
4.2.	Re-design Experiment Details to Get Better Constant Solution.....	49
4.2.1.	Using Coupling Agent for Nano-particles Surface Treatment	50
4.2.2.	Selection Specific Kind of Coupling Agent.....	50
4.2.3.	The Effect of Coupling Agent on Nano-particles.....	51
4.2.4.	Steps for Re-Designed Experiment.....	53
4.3.	Testing Result	54
Chapter 5 RESULT DISCUSSION		57
5.1	Modeling Result.....	57
5.1.1.	Periodic Model.....	57
5.1.2.	Element Size Convergence Study.....	58
5.1.3.	Effects of Nanoparticle Distribution.....	60
5.1.4.	Effects of Nanoparticle shape	65
5.1.5.	Monte Carlo Model Result.....	68
5.2.	Validation.....	69
5.3.	Conclusion	72
Chapter 6 FUTURE WORK.....		74
Chapter 7 BIBLIOGRAPHY		76

LIST OF FIGURES

FIGURE 1: ELECTROMAGNETIC WAVE OSCILLATION	14
FIGURE 2: THE ELECTROMAGNETIC WAVE TRANSMISSION MODEL FOR MATERIALS	15
FIGURE 3: SPANNER DIVIDED INTO A NUMBER OF FINITE ELEMENTS.	24
FIGURE 4: VARIOUS FINITE ELEMENTS COMMONLY AVAILABLE.....	24
FIGURE 5: SCHEMATIC DIAGRAM FOR DIELECTRIC SIMULATION.....	26
FIGURE 6: SCHEMATIC DIAGRAM FOR MAGNETIC SIMULATION	27
FIGURE 7: MAXWELL- GARNETT MODEL.....	29
FIGURE 8. DIAGRAM SHOWING SOLID98 ELEMENT	34
FIGURE 9. SCHEMATIC ILLUSTRATION OF IDEALIZED FIBER ARRAYS AND THEIR CORRESPONDING UNIT CELLS	35
FIGURE 10. CUBIC CRYSTAL DISTRIBUTION: (A) SIMPLE CUBIC (SC), (B) BODY-CENTERED CUBIC (BCC), (C) FACE-CENTERED CUBIC (FCC), (D) RANDOM DISTRIBUTED CUBIC	36
FIGURE 11. GEOMETRICAL MODEL OF DISTRIBUTION.....	37
FIGURE 12. GEOMETRICAL MODEL OF SHAPE.....	39
FIGURE 13. MONTE CARLO MODEL	40
FIGURE 14. MAGNETIZATION CURVE OF THE SYNTHESIZED $\text{Ni}_{0.5}\text{Zn}_{0.5}\text{Fe}_2\text{O}_4$ SPINEL FERRITE NANO POWDER AT ROOM TEMPERATURE.	41
FIGURE 15. B-H CURVE OF THE SYNTHESIZED $\text{Ni}_{0.5}\text{Zn}_{0.5}\text{Fe}_2\text{O}_4$ NANOPARTICLE.	42
FIGURE 16. MODEL MESH.....	43
FIGURE 17. BOUNDARY CONDITION OF PERMITTIVITY CALCULATION	44
FIGURE 18. BOUNDARY CONDITION OF PERMEABILITY CALCULATION	45
FIGURE 19. FINAL TESTING SAMPLE	47
FIGURE 23. THE EFFECT OF COUPLING AGENT ON NANOPARTICLES.....	51
FIGURE 24. THE MORPHOLOGY OF NANO-PARTICLES AFTER REACTION WITH COUPLING AGENT.	52
FIGURE 25. THE COMPARISON OF COUPLING AGENT REACTION TIME.....	52
FIGURE 26. MAGNETIZATION CURVE OF THE SYNTHESIZED EPOXY MATRIX NANOCOMPOSITES AT ROOM TEMPERATURE.	54

FIGURE 27. PERMEABILITY μ_{EFF} CURVE OF THE SYNTHESIZED EPOXY MATRIX NANOCOMPOSITES AT ROOM TEMPERATURE.	55
FIGURE 28. PERIODIC BOUNDARY CONDITION MODEL.	57
FIGURE 29. REPEATED UNIT CELL GRAPH.	58
FIGURE 30. ELEMENT SIZE CONVERGENCE GRAPH.	59
FIGURE 31. ELECTRIC FIELD DISTRIBUTION (V/CM) FOR VARIOUS CUBIC NANOPARTICLE DISTRIBUTIONS OF 8 VOL% NANOPARTICLES.	60
FIGURE 32. PERMITTIVITY VS. VOLUME FRACTION OF NANOPARTICLES FOR VARIOUS DISTRIBUTIONS AND COMPARING WITH ANALYTICAL CALCULATIONS. VOLUME FRACTION RANGING 0~1% (A) AND 0~100% (B).	62
FIGURE 33. PERMEABILITY VS. VOLUME FRACTION OF NANOPARTICLES FOR VARIOUS DISTRIBUTIONS AND COMPARING WITH ANALYTICAL CALCULATIONS. VOLUME FRACTION RANGING 0~1% (A) AND 0~100% (B).	64
FIGURE 34. MAGNETIC FIELD DISTRIBUTION (Oe) FOR VARIOUS PARTICLE SHAPES WITH BCC DISTRIBUTION.	65
FIGURE 35. PERMEABILITY VS. VOLUME FRACTION OF NANOPARTICLES FOR VARIOUS SHAPE AND COMPARING WITH ANALYTICAL CALCULATIONS.	66
FIGURE 36. MAGNETIC FIELD AND MAGNETIC FLUX OF MONTE CARLO MODEL.	68
FIGURE 37. MAGNETIC FIELD (Oe) INTERACTION IN MONTE CARLO MODEL.	68
FIGURE 38. COMPARISON OF MODELING WITH EXPERIMENTS FOR PERMEABILITY VS. MASS FRACTION OF NANOPARTICLES.	69
FIGURE 39. SCATTERING PARAMETER VS. FREQUENCY.	74

LIST OF TABLES

TABLE 1. ANSYS 3D ELEMENT TYPE	33
TABLE 2. EXPERIMENTAL DATA.	56
TABLE 3. VALIDATION OF SIMULATION RESULT WITH EXPERIMENTAL DATA.	71

ABSTRACT
ELECTRO-MAGNETIC RESPONSIVE $\text{Ni}_{0.5}\text{Zn}_{0.5}\text{Fe}_2\text{O}_4$ NANO-PARTICLE
COMPOSITE

JAIPRAKASH KANAGARAJ

2018

The purpose of this study is to simulate and synthesize a Radar (or Radiation) Absorbent Material (RAM) by using polymers and nickel zinc ferrite ($\text{Ni}_{0.5}\text{Zn}_{0.5}\text{Fe}_2\text{O}_4$) magnetic nanoparticles. There is an ardent desire in military, space and electronics for lighter, faster, cheaper and widespread bandwidth providing RAM materials. Electromagnetic property such as magnetic permeability (μ) and electric permittivity (ϵ) play a major in controlling the radiation. The appropriate combination of permeability and permittivity properties is acquired for the synthesis of RAM providing wide-ranging bandwidth. The apt property is achieved by rule of mixture, mixing of particular composition of epoxy polymer having low permeability and permittivity with the nickel zinc ferrite magnetic nanoparticle having high permeability and permittivity.

In this investigation, we studied the effective relative permeability (μ_{eff}) and permittivity (ϵ_{eff}) of $\text{Ni}_{0.5}\text{Zn}_{0.5}\text{Fe}_2\text{O}_4$ nanoparticles encapsulated within the epoxy polymer resin through Finite Element Analysis (FEA) and several various analytical experiments to verify and match both the simulation and experimental results. The FEA model was explored in two different aspect. First, shape of the nanoparticle is assumed to be spherical, cubic and bar structure. Secondly, the distribution of nanoparticle in the epoxy polymer matrix is assumed to be Simple Cubic(SC), Body Center Cubic (BCC), Face Center Cubic

(FCC) and Random distributed unit cell. The result is compared with analytic approaches (Maxwell-Garnett (M-G) theory, Bruggeman theory) and Vibrating Sample Magnetometer (VSM) experimental data.

Further, scattering parameter (S-parameter) of composite were analyzed and concluded with the best RAM material composition.

CHAPTER 1 INTRODUCTION

1.1 Significance

With the extensive proliferation of commercial, industrial and military application of Electromagnetic (EM) waves in modern technology, such as telecommunication devices, network systems and radar technology, it has attracted many concentrated research concerning in composites materials applied for the responsiveness (absorption) of electromagnetic wave.[1-6] Considerable theoretical and experimental investigation have been reported that an idea EM wave responsive material tend to possess the property of low density, high strength, high temperature resistance, strong absorption, broad bandwidth and multi-functionality.[5,7-11] For example, electromagnetic absorption is of high importance in aerospace engineering where the development of a lightweight absorbing material in a broad range of frequencies is an essential part of the Stealth Technology. An absorber soaks up the incident electromagnetic energy, thereby reducing the net energy available for reflection back to radar. In other words, the more absorptive the material is the more invisible for radar an aircraft can be. Through the current state of the stealth technology is highly classified, to the best of our knowledge today`s Radar Absorbent Materials (RAM) still suffer a trade-off between the broadband effectiveness and the absorber weight that can significantly reduce aircraft`s payload. Therefore, to date, various composite materials have been designed and applied to reach the ideal targets upon the application desire.

1.2 Background

Composite material can be designed by rule of mixture, typically it consists of two or more different type of materials, where one phase is the reinforcing phase, such as fibers,

sheets or particles and the other phase is the matrix material like metal, ceramic or polymer. The reinforcing material characteristically is a low density, high strength and stiffness material and the matrix material are more likely to have properties like corrosion, temperature or UV resistance.

Polymer Matrix Composites (PMCs) are one of the most popular composite materials due to their capability to incorporate with many different additives especially for the filler materials. The advantage of adding the filler materials can reduce the cost, alter mechanical strength, reduce mold shrinkage, control viscosity and alter surface properties.[12,13] Those properties allow PMCs to be used for a wide variety of manufacturing and industry application. In addition, polymer-matrix composites are relatively easy to manufacture in comparison to their metal, ceramic, or carbon matrix counterparts.[14] The ease at which the composites are manufactured stems from the low melting temperature that is typically found in polymer materials. However, this low melting temperature, which is very useful for manufacturing, limits the applications of polymer composites.

PMCs can be either a thermosetting or thermoplastic polymer.[15] Thermoplastics like polyethylene are easier to manufacture than thermosets, because of their ability to have higher ductility or withstand high temperatures. Thermoset polymers like epoxy are widely used as a polymer matrix, because of their good mechanical properties, corrosion resistance, adhesion properties and relatively inexpensive material cost. Epoxies are unique polymers, because of their molecular weight prior to curing lead to high molecular mobility. This high molecular mobility quickly and easily wets a filler material. Epoxy composites are widely used in conjunction with carbon fillers.

There are lots of commonly used filler materials for PMCs, like metal materials, carbon fibers, carbon nanotubes carbon vapor grown nanofibers, glass fibers and metal or ceramic particulates. Glass fibers are added to polymeric materials to improve the specific strength and since both are relatively inert materials, allows for application in corrosive environments. The addition of fillers to polymer can produce ion conducting composites,[16] impact resistant materials,[17] optical films,[18] and other enhanced property materials. [19,20]

Metal materials can be added to PMCs for different application areas, as metals are high strength, ductile and temperature resistance. The addition of a ductile metal to a ductile polymer creates a unique blend of properties for a variety of potential applications and properties. The addition of metals increases the strength of the polymer matrix, but it can also affect the electronic and optical properties. Metal-polymer composites have applications in robotics, medical devices, medical implants, actuators, and many other industrial applications. [21-24]

In this study, we investigate adding ferrite metal materials into our polymeric matrix material to enhance the composite material's ultimate electromagnetic properties such as magnetic permeability (μ) and electric permittivity (ϵ).

1.3 Literature Review

Recently, $\text{Ni}_{0.5}\text{Zn}_{0.5}\text{Fe}_2\text{O}_4$ [25-27] and [28] Fe_2O_4 nanoparticle is used as electromagnetic property enhancer play a significant role in radiation absorbent. This nanoparticle was produced by different manufacturing technique such as chemical combustion, mechanical milling, oxalate co-precipitation process etc. Wide varieties of composite material are synthesized to achieve the different range of properties. In literature

[25-27] $\text{Ni}_{0.5}\text{Zn}_{0.5}\text{Fe}_2\text{O}_4$ magnetic nanoparticle is mixed with the epoxy, Flaky FeSiAl alloy, barium lead zirconate titanate. Result shows that magnetic permeability, saturation magnetization, coercivity, remanence, electric permittivity, resistivity varies by changing the $\text{Ni}_{0.5}\text{Zn}_{0.5}\text{Fe}_2\text{O}_4$ nanoparticle content in composite mixture.

Zilli et al. [29] published an paper on Epoxy matrix composites using as filler with different weight fractions (0.03–1 wt%) of CVD grown multi-walled carbon nanotubes (MWCNTs) containing trapped iron nanoparticles. It was shown that magnetic properties are a function of the MWCNTs weight fraction, ϕ . They have found an increase in the remanent magnetization, M_R , and a decrease in the coercive field B_C with ϕ for low weight fractions ($\phi < 0.4$ wt%) that are well understood in the framework of isolated magnetic particles. However, an important change in the magnetic behavior is observed above a threshold weight fraction, where the rate of growth of M_R with ϕ abruptly increases, and B_C stops decreasing, showing a non-monotonic dependence. Both behaviors point to the agglomeration of magnetic particles in composite. So, it is very important to study the agglomeration.

Nawfal Jebbor and Seddik Bri [30] studied the effective properties of composite materials are closely related to the composition and arrangement of its constituents. Many studies and articles are actively studying the dielectric properties of heterogeneous structures with random and periodic arrangement. In the quasistatic limit, they use the finite element method as a numerical tool to evaluate the effective permittivity of two and three component composites. Two heterostructures are investigated; the first is formed by crossed dielectric cylinders in permanent contact and arranged in three layers. The cylinders are immersed in a dielectric host medium. The second structure is similar to the

first except that the tubes are covered by an interphase layer. The numerical tool used to extract the exact value of the effective permittivity takes into account all internal multipolar interactions which contribute to the polarization of the material medium. The impacts of the relative permittivity and volume fraction of cylinders, the thickness of interphase and its dielectric constant are reported. The Maxwell–Garnett theory fails to predict the effective permittivity of the studied structures for high volume fraction and permittivity contrast. To overcome this problem, an amendment was made to the McLachlan equation McQ also termed the Two Exponent Single Percolation Equation TESPE. The first exponent t is held equal to 1 and the other exponent s is depending on the volume fraction. s is calculated so that the whole values of the effective permittivity obtained by the McQ rule are exactly the same values obtained by the simulations. Finally, we obtained a chart and a model to find the values of s , a fast way that is very useful for practitioners and design engineers of composite materials. They reported that the effective permittivity ϵ_{eff} is a complex function which depends heavily on: (1) inclusion shape and their relative arrangement from the external electric field, (2) the volume fraction of inclusions, (3) the interactions between the inclusions especially for high concentrations, which is not included in the classical mixtures rules, (4) the permittivity contrast between inclusions and host media. The applicability of the effective medium approximation is valid only when the typical size of inclusions is small compared to the wavelength of the electromagnetic wave probing the heterostructure (quasistatic limit). In conclusion, they have established a series of 3D-simulations by the finite element method of dielectric composite with periodic arrangement of simple and stratified cylinders embedded in a distinct host medium. All values obtained are exact taking into account the multipolar

interactions between tubes of composite and can provide accurate information on many periodic heterostructures based on cylindrical inclusions. The Maxwell–Garnett theory can predict the effective permittivity of the studied material only in the dilute limit case. In high concentrations, the multipolar interactions become very significant and most of the mixtures rules are unable to predict the dielectric behavior of heterogeneous systems. A convenient and fast way based on the McLachlan equation was established to find all the simulation data from the values of volume fraction and permittivity contrast between inclusions and matrix. A notable time saving will be appreciated by practitioners. The effects of thickness and permittivity of the interphase were observed, practically, the thickness has no impressive effect on the effective permittivity in case of constant volume fraction and in the case of $\epsilon_2 \gg \epsilon_1$.

The concentration dependence of the remanence, the coercivity and the blocking temperature of a three-dimensional random assembly of ferromagnetic nanoparticles interacting via exchange and dipolar forces is studied by Monte Carlo simulations [31,32]. D. Kechrakos and K. N. Trohidou [32] studies the single-domain ferromagnetic particles using the Monte Carlo simulation technique. The particles have random locations, possess random uniaxial anisotropy, and are coupled through dipolar interactions. The dependence of the magnetic properties on the packing density, the size of the particles, and the temperature are examined systematically. The role of the packing geometry simple cubic (SC), face centered cubic (FCC) and the sample boundaries are discussed. The FCC packing of the particles leads to more pronounced ferromagnetic behavior than the SC packing. The sample free boundaries and the corresponding demagnetizing field have a strong effect on the remanence of the assembly while they produce a minor reduction to

the coercivity. The results from the simulations are compared with magnetic measurements on frozen ferrofluids and granular metal solids. They assumed some experiment requirement, 1) The temperature is constant. 2) Each particle possesses uniaxial anisotropy with an easy axis oriented in a random direction. 3) The particles have to a very good approximation a spherical shape. 4) The arrangement of particles in space is random. To meet the above experimental requirements, they model the particle assembly with a collection of three-dimensional classical spins located at random on the sites of a cubic lattice. Two choices for the lattice geometry (SC and FCC) are used. The magnetostatics interaction between two particles is described via a dipolar field. In a fine-particle system there are two factors determining the importance of dipolar interactions, namely, the average distance between the particles and their size. Their intention is to study independently these two factors. So, they consider two distinct types of systems. (a) Systems with particles of fixed size. (b) Systems with particles of growing size. In their model, the particle diameter increases with the metal volume fraction. They assume for simplicity that when they add more magnetic material into a sample of fixed volume, the volume of each particle increases without formation of new particles. They conclude that, in purely dipolar systems at low temperatures, both the remanence and coercivity approach zero in the limit of extreme dilution and in the limit of a fully periodic array of (nonoverlapping) spherical particles. Both magnetic properties are maximized close to the percolation threshold, due to the fractal morphology of the assembly structure. And the packing geometry of the particles has a small effect on the magnetization and coercivity at very low temperatures. FCC packing produces up to 10% higher values than the SC packing for systems with moderate interactions.

Morihiko Matsumoto and Yoshimori Miyata [33] designed a soft magnetic material with flaky thin amorphous metal particles about 2 μm thick and that are aligned in polymer in the direction perpendicular to electromagnetic wave propagation. They have stated that material yields a permeability two to three times higher than the spinel-type ferrite system in the quasi-microwave band. Similarly, as in literature [34].

Jun Zhang et al. [35] report a preparation of high-quality cubic PbTe nanocrystals and their assembly into both square-array, two-dimensional patterns and three-dimensional simple cubic super crystals. The influence of oleylamine in the nanocrystal synthesis and core-shell formation through an anion-exchange mechanism was also studied. The simple cubic super crystals together with two-dimensional assembly patterns containing PbTe nanocubes and their core-shell building blocks were examined using TEM, SEM, AFM, XRD, SAXS, and FTIR. Such super crystals consisting of cubic structural building blocks may allow engineering of more complex materials from which novel properties may emerge. Self-Assembly of Nanocubes. On a copper grid coated with Formvar/carbon (product code: 01801, from Ted Pella Inc.), nanocubes could be assembled via two pathways, designated as “fast” and “slow”. For the fast process, the grid was horizontally placed on a piece of filter paper so that the excess solvent was rapidly absorbed by the paper as soon as the nanocube suspension was dropped using a pipette, leaving the NCs deposited on the grid. For the slow process, the grid was vertically hung by a pair of self-closing TEM tweezers and submerged in a suspension of PbTe nanocubes in a vial. The solvent was allowed to naturally evaporate until the level of the colloidal solution was below the TEM grid. In this way, NCs were slowly deposited on the grid at the interface of the solvent surface, TEM grid surface, and air. It should be pointed out that the

concentration of the nanocube suspension is an additional factor that controls the quality of assembled pattern. Simple cubic of various nanocubes could also be built on a solid substrate, such as a silicon wafer or kapton film. Typically, a sufficient amount of concentrated nanocube suspension was prepared using 95 wt % of anhydrous hexane and 5 wt % of anhydrous ethanol. This colloidal suspension was transferred into a vial containing a piece of substrate horizontally placed on the bottom. The system was placed in an ambient environment until all of the solvent evaporated “naturally”, leaving the nanocubes assembled onto the surface of the substrate. This study may be useful in our model preparation, formation of $\text{Ni}_{0.5}\text{Zn}_{0.5}\text{Fe}_2\text{O}_4$ nanoparticle distributed in epoxy such as SC, BCC, FCC periodic pattern.

1.4 Motivation

Since, there is a ton of literature on this field but only some article inspired me to do research. Firstly, Zilli et al. [29] conclude that the iron nanoparticle are trapped inside the epoxy matrix, their property may varied by the agglomeration of magnetic iron nanoparticle. Secondly, Nawfal Jebbor and Seddik Bri [30] reported that the effective permittivity ϵ_{eff} is a complex function which depends heavily on: (1) inclusion shape and their relative arrangement from the external electric field, (2) the volume fraction of inclusions, (3) the interactions between the inclusions especially for high concentrations, which is not included in the classical mixtures rules, (4) the permittivity contrast between inclusions and host media.

On the other hand, the actual absorbers on the market are not able to provide the wide range bandwidth material with considerable price, substantial weight, low integrity to the whole structure of the devices, and a limited range of frequencies are all factors that

prevent the application of these materials in the aeronautics industry. To address this challenge, Nano-size ferromagnetic particles have an enormous potential to be used as onboard microwave absorbers. Recently, due to the possibility of producing ferromagnetic nanoparticles, research on these particles become of a great interest [36].

More over $\text{Ni}_{0.5}\text{Zn}_{0.5}\text{Fe}_2\text{O}_4$ Nanoparticle shows its ability of producing wide range of electromagnetic radiation absorbent property. It is crucial to understand how the metallic nanoparticles are behaving inside electromagnetic environment. So, having a good understanding of electromagnetic property of ferromagnetic nanoparticle would be a must.

More specifically, a new foundational fabrication of electromagnetic-responsive materials is being proposed which would be more economical and more processable.

1.5 Objective

The main theme of this thesis is to produce a radiation absorbent material (RAM).

Various subdivision of research has been conducted,

- Development of polymer-based Nanocomposite for radiation absorbent material is reviewed and try to understand the EM wave absorption mechanism.
- Synthesis of $\text{Ni}_{0.5}\text{Zn}_{0.5}\text{Fe}_2\text{O}_4$ encapsulated epoxy composite having different weight ratio of Nanoparticle content.
- Electromagnetic properties of synthesized composite were measured by appropriate experiment.
- Comparison of inclusion shape and their relative arrangement/distribution of Nanoparticle in epoxy is simulate using the ANSYS software.
- The volume fraction of inclusions and interactions between the inclusions which is not included in the classical mixtures rules is studied using the simulated results.

- Validation of simulation results with the experimental results.
- Test the scattering parameter of composite and conclude.

CHAPTER 2 FUNDAMENTAL OF EM WAVE ABSORPTION

2.1. Maxwell's Equation

Whenever an electromagnetic wave strikes a conductive object, electrons are excited and surface current is generated. The surface currents transmit electromagnetic energy, which is temporarily entrapped on the objective's surface. The energy will be absorbed or re-radiated by the objective.

Electromagnetic waves can be analyzed by solving Maxwell's equations, which are governed by four equations[37]. They are usually stated as Ampere's Law, Faraday's Law, Poisson's Law and the condition of solenoid magnetic flux density:

$$\nabla \times \mathbf{E} = -\mu_0 \frac{\partial \mathbf{H}}{\partial t} \quad (2-1)$$

$$\nabla \times \mathbf{H} = \mathbf{J} + \frac{\partial \mathbf{D}}{\partial t} \quad (2-2)$$

$$\nabla \cdot \mathbf{D} = \rho \quad (2-3)$$

$$\nabla \cdot \mathbf{B} = 0 \quad (2-4)$$

where:

H is the magnetic field intensity (A/m) or (Oe) in CGS unit

B is the magnetic induction flux (T or Wb/m^2) or (Gauss) in CGS unit

D the electric displacement (C/m^2) or C/cm^2) in CGS unit

E the electric field intensity (V/m) or (V/cm) in CGS unit

J the electric current density (A/m^2)

ρ the electric charge density (C/m^3)

$\mu^0 = 0.4 \times 10^{-6}$ H/m is permeability of vacuum.

Solutions of all electromagnetic problems incorporate the following material properties related equations named constitutive equations:

$$\mathbf{D} = \epsilon_0 \epsilon_r \mathbf{E} \quad (\text{SI units}) \quad (2-5.a)$$

$$\mathbf{D} = \epsilon \mathbf{E} \quad (\text{Gaussian units}) \quad (2-5.b)$$

$$\mathbf{B} = \mu_0 \mu_r \mathbf{H} \quad (\text{SI units}) \quad (2-6.a)$$

$$\mathbf{B} = \mu \mathbf{H} \quad (\text{Gaussian units}) \quad (2-6.b)$$

$$\mathbf{J} = \sigma \mathbf{E} \quad (2-7)$$

where:

$\epsilon_0 = 8.854 \times 10^{-12} \text{F/m}$ is the permittivity of vacuum.

$\mu_0 = 4\pi \times 10^{-7} \text{H/m}$ is the permeability of vacuum.

ϵ_r, ϵ is the complex relative permittivity and permittivity.

μ_r, μ is the complex relative permeability and permeability.

σ is the conductive of material (S/m).

Hence, σ , μ_r and ϵ_r these three properties govern the propagation of electromagnetic waves through the material. In electromagnetism, permeability is the measure of the ability of a material to support the formation of a magnetic field within itself, which could be expressed the degree of magnetization that a material obtains in response to an applied magnetic field. Permittivity is the measure of the resistance that is encountered when forming an electric field in a medium. In other words, permittivity is the measure of how an electric field affects, and is affected by, a dielectric medium.

Also, the relative complex permittivity and permeability can be written as:

$$\epsilon_r = \frac{\epsilon}{\epsilon_0} = \epsilon' + \epsilon'' \quad (2-8)$$

$$\mu_r = \frac{\mu}{\mu_0} = \mu' + \mu'' \quad (2-9)$$

The magnitude ratio of E to H is the wave impedance Z:

$$\frac{E}{H} = \sqrt{\frac{\mu}{\epsilon}} = Z \quad (2-10)$$

This shows that the impedance is a function of the permeability and permittivity of the medium that wave propagates in. In the case of normalizing impedance where the wave impedance is divided by the impedance of air, Z_0 , the above equation (10) becomes:

$$\frac{Z}{Z_0} = \frac{\sqrt{\frac{\mu}{\epsilon}}}{\sqrt{\frac{\mu_0}{\epsilon_0}}} = \sqrt{\frac{\mu_r}{\epsilon_r}} \quad (2-11)$$

In summary, the electromagnetic wave equation is derived from Maxwell's equations and demonstrates that an electromagnetic wave has both magnetic and electric components (perpendicular to each other, oscillating in the time and space phase). The ratio of E and H is the wave impedance associated with the permeability and permittivity of medium. The far field is called to the region greater than $\lambda/2\pi$ (λ is the wavelength as shown in Figure 1). The wave is known to be a plane wave as in the far field, all radiated EMI waves essentially lose their curvature, and the surface containing E and H becomes a plane.

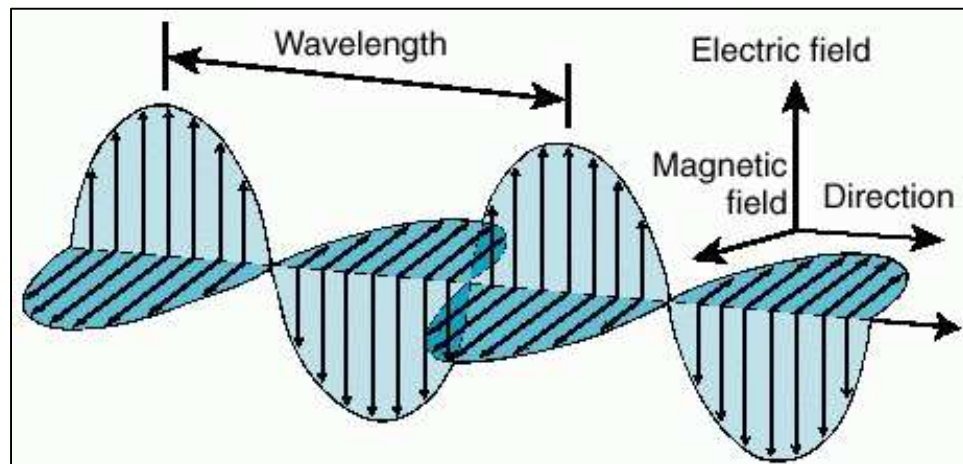


Figure 1: Electromagnetic Wave Oscillation

2.2. EM Wave Absorption Ability

EM wave absorption is the process of the energy of electromagnetic wave being depleted and then transformed into other energy (e.g., thermal energy) other than the wave being reflected or permeated through the materials[38,39]. There are three processes included reflection, absorption and penetration when an incident electromagnetic wave through an EM absorption material. A conductive material is the best candidate for reflection as its shielding is based on mobile charge carriers (electrons) in the material. These mobile charges carriers generate an impedance mismatch between free space wave impedance and essential impedance of the shield. Because of this mismatch, a large part of incident field is reflected like the Figure 2 shows bellowed.

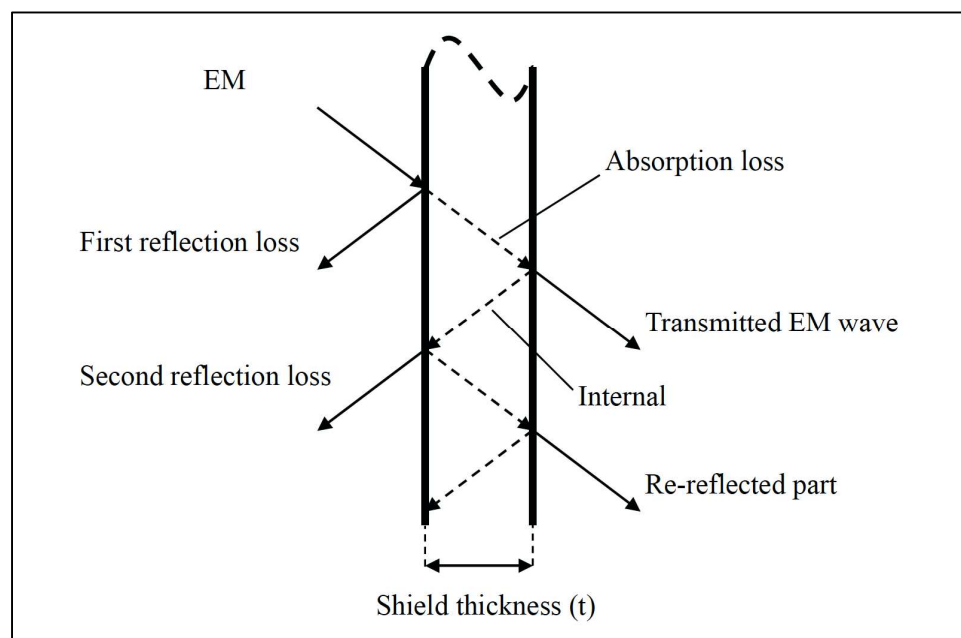


Figure 2: The electromagnetic wave transmission model for materials

It has been reported that as ideal EM wave absorption materials, they must satisfy two prerequisites: 1). To prevent wave being reflected, the impedance is required to match between free space and the material surface, which needs the complex permittivity close

to complex permeability. 2). Materials possessing strong magnetic and dielectric loss guarantee the absorbing incident waves as many as possible inside of the absorbers.[40]

When a wave interacts with the surface of an object, part would be reflected and part would be transmitted. The reflection depends on the material and frequency of propagation. The reflection coefficient (R) for the normal incident would be calculated by the normalized impedance Z/Z_0 :

$$\mathbf{R} = \frac{\frac{z}{z_0}-1}{\frac{z}{z_0}+1} \quad (2-12)$$

R is a complex number (normalized impedance is a function of relative permittivity and permeability). Generally, The EM wave absorption ability was often indicated by the reflection loss (R_L):

$$\mathbf{R_L(dB)} = 20 \log|\mathbf{R}| \quad (2-13)$$

Wave impedance presents how the relative permeability and permittivity (material properties) can affect the reflection loss (R_L). Value of 10 and 20 dB for R_L represent that 90% and 99% EM waves are absorbed by the absorbers respectively.[38]

2.3. EM Wave Absorption Mechanism

There are two mainly mechanism regarding the process of energy depletion within the EM absorption materials: Dielectric loss and magnetic loss.

2.3.1. Magnetic Loss Mechanism

Eddy current loss, magnetic hysteresis loss and residual loss are mainly three energy loss when magnetic material interacting with induced electromagnetic waves.[41] According to Legg's equation, the magnetic loss at low frequency and low magnetic flux density can be expressed as[42]:

$$\frac{2\pi\text{tg}\delta_m}{\mu} = e\mathbf{f} + a\mathbf{B} + c \quad (2-14)$$

Where e , a , c , μ , $\text{tg}\delta_m$ and B represent eddy current loss coefficient, magnetic hysteresis coefficient, residual loss, permeability, magnetic loss tangent (the ratio of image part of dielectric property over real part of that) and magnetic flux density respectively.

2.3.1.1. Eddy Current Loss

Eddy current is electric current induced within conductors by an alternating magnetic field, which would dissipate the energy, that is, eddy current loss. Eddy current loss coefficient, e can represent the eddy current loss at low frequency and low magnetic flux density. For a sheet with a thickness of d and electric conductivity of σ , the eddy current loss coefficient can be expressed as[41]:

$$e = \frac{4\pi^2\mu_0 d^2 \sigma}{3} \quad (2-15)$$

It is apparent that in order to increase the eddy current loss, the material must possess large thickness and electric conductivity. However, there is another problem that the permeability at high frequency would be unstable when the material with high electric conductivity, which restricts its application of high frequency.[43] On the other hand, the dependence of d and σ on the eddy current loss was similar to which at high frequency even the Eq.3 was derived at low frequency.[44] Additionally, other factors, such as orientation, grain size, surface roughness, morphology of material would also affect the eddy current loss.[41,45,46]

2.3.1.2. Magnetic Hysteresis Loss

The irreversible domain movement and magnetic moment rotation of magnetic material induces the magnetic hysteresis loss. At low magnetic flux density, the magnetic hysteresis coefficient could be expressed as[41]:

$$a = \frac{8b}{3\mu_0\mu^3} \quad (2-16)$$

Where b , μ_0 , μ represent the Rayleigh constant, vacuum permeability and permeability of material. According to Eq.4, the magnetic properties of material, including the Rayleigh constant and permeability of material, mainly determines the magnitude of magnetic hysteresis loss.

2.3.1.3. Residual Loss

The magnetic loss except eddy current loss and magnetic hysteresis loss is called as residual loss, which is determined by the amplitude of alternating magnetic field and relaxation time of material. At low frequency, magnetic aftereffect loss, such as thermal fluctuation, the hysteresis of electrons and ions moving to equilibrium position relative to the diffusion of applied magnetic field, causes the residual loss.[41] For high frequency, the residual loss is determined by size resonance, ferromagnetic resonance, natural resonance and domain wall resonance, which suggests that satisfactory magnetic loss could be achieved by controlling the particle size, anisotropy of magnetic material and other magnetic properties.[38,41,47,48]

2.3.2. Dielectric Loss

Dielectric loss is the electric energy dissipated and then transformed into heat energy when an EM wave induced into a dielectric material. The mechanism of dielectric

loss include conductance loss ($tg\delta_e$), dielectric relaxation loss ($tg\delta_{rel}$), resonance loss ($tg\delta_{res}$) and so on.[49,50]

2.3.2.1. Conductance Loss

Conductance current would be produced when a changing electric field acted on wave absorption material which possess certain electric conductivity, which would dissipate the energy in the form of heat energy. Hence, electric conductivity of material determines the conductance loss, which could be expressed by conductance loss tangent, $tg\delta_c$ [49]:

$$Tg\delta_c = 1.8 \times 10^{10} \frac{\sigma}{f\epsilon_r} \quad (2-17)$$

2.3.2.2. Dielectric Relaxation Loss

Material would be polarized under the electric field and the dielectric relaxation loss would be produced under the situation that the change of polarization is slower than that of electric field. The polarization mainly includes thermal ion polarization, dipole rotation polarization, electronic displacement polarization, ion polarization and so on. The electronic displacement and ion polarizations produce energy loss just at ultra-high frequency since the time is very short just about 10^{-15} - 10^{-14} s. However, for thermal ion and dipole rotation polarizations, the time is about 10^{-8} - 10^{-2} s.[51] As a result, the thermal ion and dipole rotation polarizations play the greatest role in relaxation loss at high frequency. Debye equation can be used to calculate the dielectric relaxation loss tangent $tg\delta_{rel}$ [49]:

$$tg\delta_{rel} = \frac{\epsilon_r(\omega)}{\epsilon_r(\omega)} = \frac{(\epsilon_{rs} - \epsilon_{r\infty}) \omega \tau}{\epsilon_{rs} + \epsilon_{r\infty} \omega^2 \tau^2} \quad (2-18)$$

where ϵ_{rs} , $\epsilon_{r\infty}$ and τ represent the permittivity at frequency approaching to zero and infinity, and relaxation time.

2.3.2.3. Resonance Loss and Other Loss

Resonance effect causes the resonance loss, which induced by the vibration of atoms, ions, or electrons inside of the wave absorption material at the scope of infrared to ultraviolet frequency. There also are other mechanism to induce the energy loss.[49] For example, Gentner et al.[50] demonstrated that the domain-wall motion could cause dielectric loss in ferroelectric ceramics: the domain-wall motion was ascribed to point defects at low frequency and the reflection of thermal lattice wave at high frequency.

2.4. Influence Factors for Electromagnetic Wave Absorption

According to the electromagnetic wave absorption mechanism, the electromagnetic wave absorption property of material is greatly influenced by its electrical and magnetic properties, size, morphology and structure. Therefore, all parameters must be well designed to reach the impedance matching for gaining the better electromagnetic wave absorption property of material. There are some main factors affecting wave absorption property of material.

2.4.1. Complex Permittivity

Relative complex permittivity is the first electric parameter of material. It is concluded that, from the dielectric loss tangent, $tg\delta_d = \frac{\xi}{\epsilon}$, the bigger the image part of complex permittivity, the better the wave absorption effect. As a result, materials with high permittivity are preferred to act as the EM wave absorbers. But, on the other hand, the reflection part of wave is relatively large for the material with too high permittivity.[10] Hence, we must choose a proper permittivity according to the practical need. If the

component is the matrix, like polymer, the material with low dielectric loss is better for the wave absorption property, which makes more waves transmit into the absorber.[52]

2.4.2. Complex Permeability

The other basic parameter determining the electromagnetic wave absorption property of material is complex permeability. From the magnetic loss tangent, $tg\delta_m = \frac{\mu''}{\mu'}$ and the magnetic loss mechanism, we also can deduce that the bigger the image part and the smaller the real part of complex permeability, the larger the magnetic loss for wave absorption material. However, according to the principle of impedance match, when the permeability is equal to the permittivity of material, there is no reflection and the electromagnetic wave absorption effect is the best.[53]

2.4.3. Electric Conductivity

From the above wave absorption mechanisms, we know that increasing the conductivity is accompanied with the increasing eddy current loss and conductance loss. But, on the other hand, the impedance of material with high conductivity is relatively small comparing to that of air, which leads the skin depth is very small and thus nearly most of electromagnetic wave would be reflected instead of absorbed.[54] Based on the study of simulation on wave absorption of Nanostructured magnetic metallic film conducted by Deng et al. [54], it has been found that the relaxed FeCoNbZrDy nanocrystalline film exhibited maximum wave absorption (-30 dB) at 10 S/cm, but the wave absorption properties decreased with the increase of conductivity; for resonant FeCoNbZr nanocrystalline film, the wave absorbing intensities increased firstly and decreased then with the increase of conductivity increasing. According to this, we could conclude that a

proper electric conductivity of material must be designed to get better wave absorption effect.

2.4.4. Nano-effect Morphology

Due to the particular size, surface and quantum tunnel effect, nanomaterial possesses excellent electric, magnetic and optic properties. For example, the density of material with Nano-dimension is relatively lower than that of bulk one; it is endowed with large specific surface area, and a large number of active atoms at its surface, which has large interface dielectric loss caused by interface polarization. On the other hand, the effective permeability decreases at high frequencies when the conductivity of metallic magnetic material is too high due to eddy current loss induced by electromagnetic waves. The eddy current loss can be induced to enhance the stability of wave absorption property if the particle size is below the skin depth. Generally, the skin depth of material is about $1\mu\text{m}$ at microwave frequencies (10GHz), and as a result, nanoparticle will possess excellent electromagnetic wave absorption property at broad frequencies[55]. Moreover, magnetic material become monodomain relative to multidomain in the bulk one when the diameter is below a critical size, like cylindrical Fe and Ni rods, the critical diameter is 23nm and 52 nm respectively.[56] For a multidomain magnet, the magnetization process contains two parts: the rotation of magnetic moment and movement of domain wall, in which the latter makes the former more convenient by changing the volume of domain. But in terms of the monodomain, materials are endowed with higher coercive force and larger magnetic hysteresis loss since there is no movement of domain wall.

2.4.5 Structure of Material

It is difficult to achieve the impedance match and broad frequencies wave absorption for single dielectric or magnetic material. Therefore, it is necessary to design materials with the different structures to get optimal electromagnetic wave absorption properties, including blends with different dielectric and magnetic materials, multilayer structures, core/shell structures and so on. The most convenient method to prepare composites is physical blend, which is mixing directly dielectric materials with magnetic particles. The second method is multilayer structure including impedance matching layer, electromagnetic wave loss layer and reflective layer, in which the impedance layer can transmit the electromagnetic wave without reflection by adjusting the complex permittivity and permeability of material. In this way, we could match the wave impedance, enhance electromagnetic wave absorption ability and broaden the absorption frequencies of wave absorption material. The role of the electromagnetic wave loss layer composing of high dielectric or magnetic loss material is depleted the electromagnetic wave. In terms of the reflective layer is to make a small quantity of transmission wave back to the wave loss layer. The other approach to the impedance match is combing the two methods above. This is not only the multilayer structure of electric and magnetic materials, but also the nanoparticles dispersing homogenously inside the wave absorption materials, which leads the material with core/shell structure has the potential to exhibit the excellent electromagnetic wave absorption ability.

2.5. Finite Element Analysis (FEA) in ANSYS

Finite element analysis is a method of solving, usually approximately, certain problems in engineering and science. It is used mainly for problems for which no exact

solution, expressible in some mathematical form, is available. As such, it is a numerical rather than an analytical method. Methods of this type are needed because analytical methods cannot cope with the real, complicated problems that are met with in engineering. FEA is essentially a piece-wise process. It can be applied to one-dimensional problems, but more usually there is an area or volume within which the solution is required. This is split up into a number of smaller areas or volumes, which are called finite elements. Figure 3 shows a two-dimensional model of a spanner that has been so divided: the process is called discretization, and the assembly of elements is called a mesh.

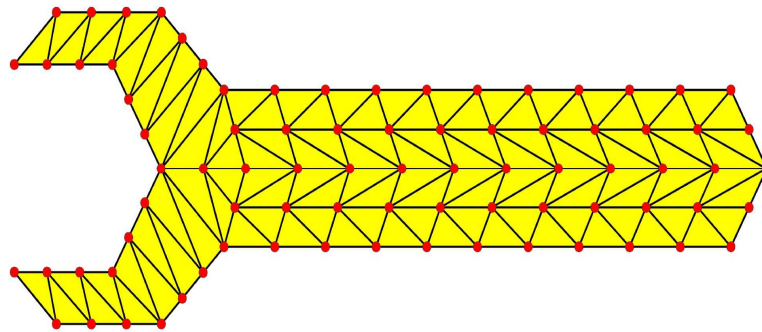


Figure 3: Spanner divided into a number of finite elements.

Elements can be of various shapes (as shown in Figure 4), in two dimensions, quadrilateral or triangular, and in three-dimensions, brick-shaped (hexahedral), wedge-shaped (pentahedral) or tetrahedral. This is, of course, not an exhaustive list.

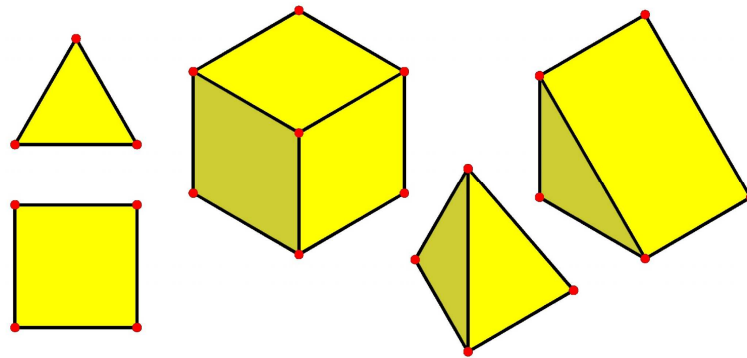


Figure 4: Various finite elements commonly available.

In our model, a few statements are made before the constitutive equation is adopted.

- First, we assume that at a given point both phases are linear dielectrics.
- An assumption of perfect interfaces between Nano-particle and epoxy is made where voids and interfacial phases are absent.
- Grain boundary and grain size effect are not considered since the model has constitutive equations making allowances for this information.
- Finally, temperature is assumed to be constant.

2.5.1. Dielectric Model

Based on the assumption above, the model is constructed starting from the one of the constitutive equation (2-5) introduced earlier:

$$\mathbf{D} = \epsilon_0 \epsilon_r \mathbf{E} \quad (2-5)$$

From simulation, we can obtain E and D. From equation (2-5), we can calculate the permittivity of our composite material, which is one of our required parameter for EM wave absorption. Hence, the material is exposed to a static electric field, which is generated by applying voltage $\varphi = \varphi_2$ across the opposite faces of the cube, and other faces of the cube meet the requirement of $\varphi = \varphi_1 = 0$. After meshing the material, from solution we could get the volume V, electric field intensity E and electric displacement D of each element. Similarly, we could apply a static electric field in other two directions to get their E and D respectively.

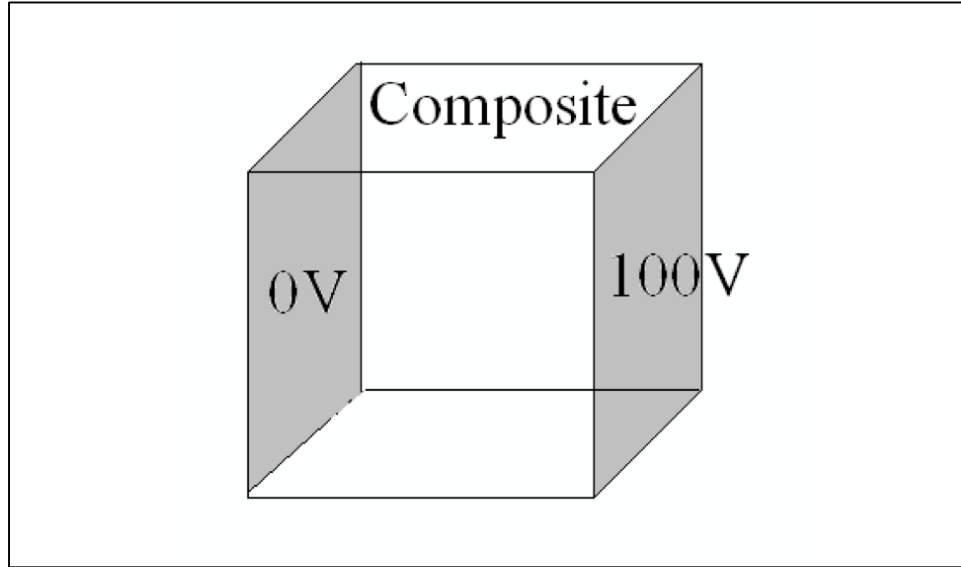


Figure 5: Schematic diagram for dielectric simulation

After getting E and D of each element, we could use the equations bellowed to derive permittivity in the corresponding direction:

$$\mathbf{D}_{rx} = \frac{D_{ri1}V_{i1} + D_{ri2}V_{i2} + D_{ri3}V_{i3} + \dots + D_{rij}V_{ij}}{V_{i1} + V_{i2} + V_{i3} + \dots + V_{ij}} = \frac{\sum_{j=1}^n D_{rij}V_j}{v} \quad (2-19)$$

$$\mathbf{E}_{rx} = \frac{E_{ri1}V_{i1} + E_{ri2}V_{i2} + E_{ri3}V_{i3} + \dots + E_{rij}V_{ij}}{V_{i1} + V_{i2} + V_{i3} + \dots + V_{ij}} = \frac{\sum_{j=1}^n E_{rij}V_j}{v} \quad (2-20)$$

$$\boldsymbol{\epsilon}_{rx} = \frac{1}{\epsilon_0} \frac{D_{rx}}{E_{rx}} = \frac{1}{\epsilon_0} \frac{\sum_{j=1}^n D_{rij}V_j}{\sum_{j=1}^n E_{rij}V_j} \quad (2-21)$$

Using the same method, we could compute permittivity in other two directions and finally averaged all the three permittivity's in x, y and z direction to gain the effective permittivity of our composites:

$$\boldsymbol{\epsilon}_r = \frac{\boldsymbol{\epsilon}_{rx} + \boldsymbol{\epsilon}_{ry} + \boldsymbol{\epsilon}_{rz}}{3} \quad (2-22)$$

2.5.2. Magnetic Model

Similarly, the simulation to obtain effective permeability is also using constitutive equation, which applies scalar magnetic field on opposite face of model.

$$\mathbf{B} = \mu_0 \mu_r \mathbf{H} \quad (2-6)$$

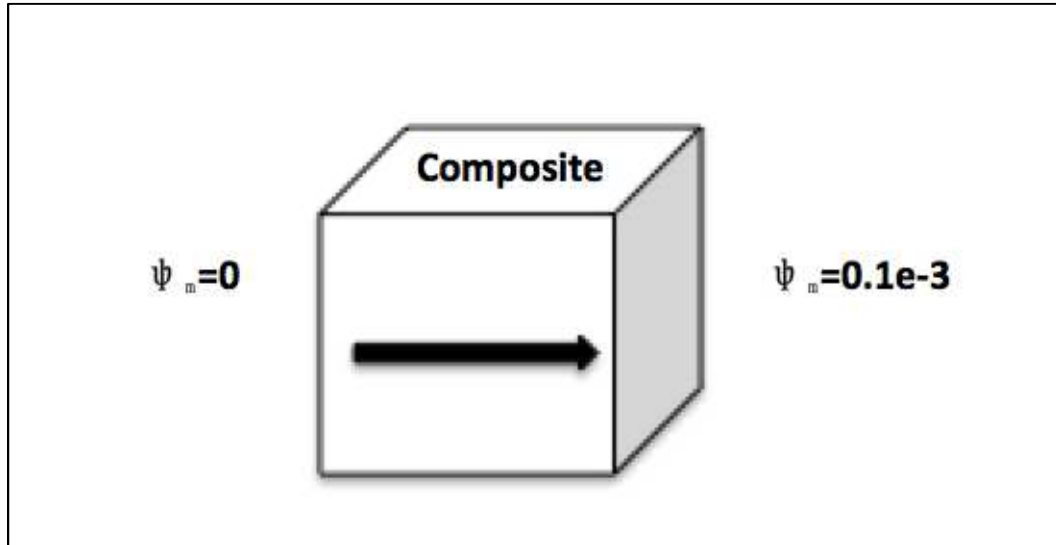


Figure 6: Schematic diagram for magnetic simulation

After getting B and H of each element from solution, we could use the equations bellowed to derive permeability in the corresponding direction:

$$\mathbf{B}_{rx} = \frac{B_{r11}V_{i1} + B_{r12}V_{i2} + B_{r13}V_{i3} + \dots + B_{rij}V_{ij}}{V_{i1} + V_{i2} + V_{i3} + \dots + V_{ij}} = \frac{\sum_{j=1}^n B_{rij}V_j}{v} \quad (2-23)$$

$$\mathbf{H}_{rx} = \frac{H_{r11}V_{i1} + H_{r12}V_{i2} + H_{r13}V_{i3} + \dots + H_{rij}V_{ij}}{V_{i1} + V_{i2} + V_{i3} + \dots + V_{ij}} = \frac{\sum_{j=1}^n H_{rij}V_j}{v} \quad (2-24)$$

$$\mu_{rx} = \frac{1}{\mu_0} \frac{B_{rx}}{H_{rx}} = \frac{1}{\mu_0} \frac{\sum_{j=1}^n B_{rij}V_j}{\sum_{j=1}^n H_{rij}V_j} \quad (2-25)$$

$$\mu_r = \frac{\mu_{rx} + \mu_{ry} + \mu_{rz}}{3} \quad (2-26)$$

2.6. Review of Conventional Analytic Theories for the Properties of a Dielectric composite or a Magnetic Composite

A brief summary of previous published analytic theories for describing the relative effective permittivity of a 2-phase composite with dielectric or magnetic inclusions in a non-electromagnetically active matrix will be given in this section. There are several famous theories like Maxwell-Garnett (M-G) theory, nonsymmetric- Bruggeman (or simply Bruggeman) theory, Poon-Shin (P-S) theory, Landauer theory and Rayleigh theory.

2.6.1. Maxwell-Garnett (M-G) Theory

The M-G theory was proposed based on a model as depicted in Figure 7. A dielectric sphere having a linear and isotropic relative permittivity ϵ is embedded in a matrix. The whole system is placed in an environment of a uniform external electric field \vec{E}_m . Hence the M-G theory can be expressed as the equation bellowed:

$$\epsilon_{eff} = \epsilon_1 + 3f\epsilon_1 \frac{\epsilon_2 - \epsilon_1}{\epsilon_2 + 2\epsilon_1 - f(\epsilon_2 - \epsilon_1)} \quad (2-27)$$

Similarly, for the whole system is placed in an environment where uniform magnetic field is applied externally.

$$\mu_{eff} = \mu_1 + 3f\mu_1 \frac{\mu_2 - \mu_1}{\mu_2 + 2\mu_1 - f(\mu_2 - \mu_1)} \quad (2-28)$$

Where:

ϵ_1, μ_1 – permittivity and permeability of material 1 (matrix)

ϵ_2, μ_2 – permittivity and permeability of material 2 (inclusion)

f – volume fraction of inclusion added in matrix

But the M-G theory has some limitations, as the model designed to have one sphere in an infinitely large matrix is over-simplified. In a real case, there are much more

inclusions separated by finite distances such that the electrical field generated from individual inclusions would superimpose with each other and the inclusion shape is unlikely to be spherical in reality also the size of the matrix is finite such that edge effect would occur. Consequently, the M-G theory can only be a fairly good approximation when f volume fraction coefficient is small enough (dilute case) and the inclusion shape is approximately spherical.[57]

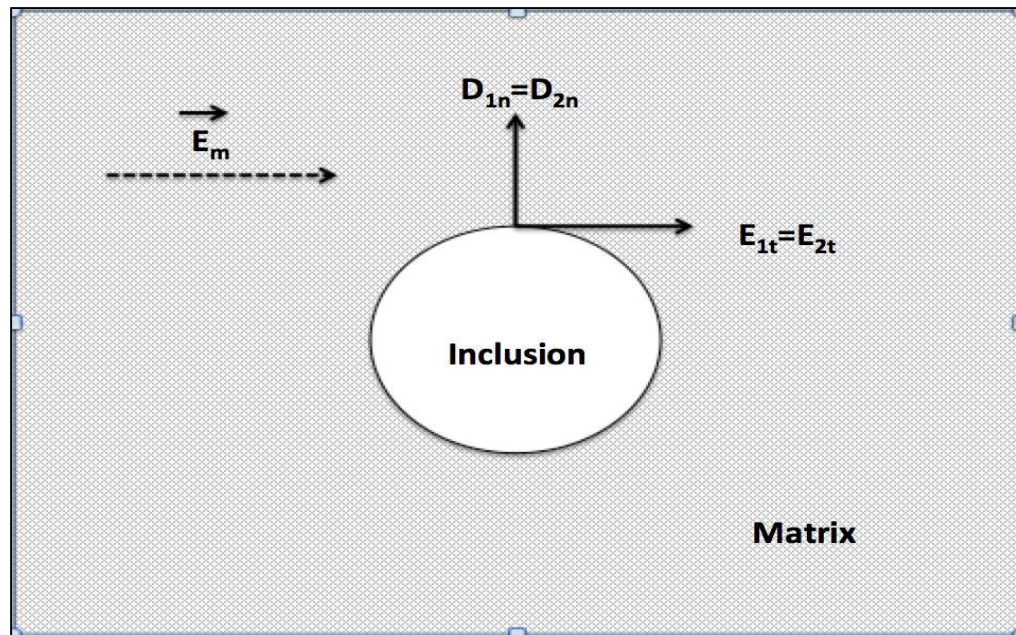


Figure 7: Maxwell- Garnett Model

2.6.2. Bruggeman Theory

Bruggeman modified the M-G formula by introducing a differentially mixing process, where infinitesimal spherical inclusions are added progressively and the permittivity of the matrix is modified cumulatively. At a particular moment, the composite containing inclusions with a volume fraction is regarded as a homogeneous substance and is thus regarded as a matrix. The Bruggeman model is considered to be better than the M-G model. First, the employment of concurrent accumulative modification of the matrix

properties with addition of inclusions released the geometrical constraint, which limits the maximum inclusion volume fraction as in the case of the M-G one. Second, the approach attempts to include the influence of all the inclusions on the matrix (and hence the composite), such that the effect due to the interaction between the inclusions located closely is considered to some extent. As such, the predicted result of ε_{eff} , μ_{eff} in Equation (2-29,30) is found to be closer to the experimental one than that predicted by the M-G theory. This is particularly true in the region of high inclusion volume fraction. Normally, the result of the Bruggeman theory is higher than that of the M-G theory.

$$(1 - f) \frac{\varepsilon_1 - \varepsilon_{eff}}{\varepsilon_1 + 2\varepsilon_{eff}} + f \frac{\varepsilon_2 - \varepsilon_{eff}}{\varepsilon_2 + 2\varepsilon_{eff}} = 0 \quad (2-29)$$

$$(1 - f) \frac{\mu_1 - \mu_{eff}}{\mu_1 + 2\mu_{eff}} + f \frac{\mu_2 - \mu_{eff}}{\mu_2 + 2\mu_{eff}} = 0 \quad (2-30)$$

On the other hand, in Bruggeman's approach, the inclusions are added in a way that as if they are "dissolved" in the matrix in successive differential steps, such that the substance constructed would be a continuous medium but cannot reproduce the real material structure. [58] In particular, the boundaries between the inclusions and the matrix in the real system do not appear in the model. This is why the theory is also referred to as the "effective medium theory (EMT)". One would therefore expect that the ε_{eff} , μ_{eff} value predicted with this theory would deviate more or less from the true one, especially when the inclusion volume fraction is large. In addition, the model does not reflect the influences due to some other factors, such as the inclusion shape and their distribution, which are the difficulties common to most analytic theories where exact formulation describing every detail of a real system is not easily established.

CHAPTER 3 FEA MODELING CONSTRUCTION

3.1. Typical FEA Process

A. Building up a Model:

This is the most time-consuming part in an analysis. It involves the construction of a structure according to the real system. In the present study, the model is made to contain inclusions of specific shape(s) distributed in a certain pattern. A mechanism is introduced to generate a magnetic field. In addition, the element types, meshing size, element real constants and material prosperities are specified.

B. Meshing:

The model is then meshed by dividing it into several elements. The vertices of the elements are defined as nodes. The size of the elements should be appropriately selected, such that the nodes of two adjacent elements can properly match. If the elements are too coarse, the model would deviate significantly from the real system. Many details of the system cannot be reproduced. This induces some errors in the calculation. If the elements are too fine, the node number may be too large for the computer to handle.

C. Applying Loads:

In this step, loads such as forces, stresses, electric or magnetic field are applied to a system under investigation. In addition, the degree of the freedom (DOF), constraints, boundary conditions and symmetry are required to be specified.

D. Obtaining Solution:

Numerical calculation is then performed, say by sending the problem to built-in processor of a software. A solution will be obtained if the problem is successfully solved.

E. Reviewing Results:

There are two types of calculated results, namely, the reckoned one and the derived one. The former refers to the data obtained directly from the calculations. In our case, they are the nodal magnetic field distribution. The derived data include induction field distribution, element averages of H and B , and element volumes etc. These results can be plotted as a vector diagram or a contour diagram. The numerical values can also be provided in a tabulated format. Further calculations can be performed by some build-in function of the software.

For performing FEA model in this research, the commercial source code ANSYS 14.5 was used. Firstly, we calculate the values of μ_{eff} of composites containing magnetic inclusions by using model shown in Fig.6, which a constant magnetic scalar potential drop is applied. For calculating ε_{eff} of composite containing dielectric inclusions, the model shown in Fig.5 is used where a constant voltage is applied. Based on the principle of equivalency as mentioned in Section 2.5 the value of μ_{eff} derived is shown to be the same that of ε_{eff} of a composite with the same geometrical structure.

3.2 Introduction of Electromagnetic Element in ANSYS

ANSYS Element Library has more than 100 element types including the 26 types of electromagnetic elements (2D and 3D solid element). In our research, we mainly to select the 3D solid element for our simulation based from the table showed below:

Table 1. ANSYS 3D Element Type

Element	Dimensional Type	Shape and Nodes	Degree of Freedom
SOLID5	3D	Hexahedron, 8 Nodes	Each Node has 6 DOF, Displacement, Temperature, Voltage, Magnetic Scalar Potential
SOLID96	3D	Hexahedron, 8 Nodes	Magnetic Scalar Potential
SOLID97	3D	Hexahedron, 8 Nodes	Magnetic Vector Potential, Voltage, Current Flow, Electromotive Force
SOLID98	3D	Tetrahedron, 10 Nodes`	Each Node has 6 DOF, Displacement, Temperature, Voltage, Magnetic Scalar Potential
SOLID122	3D	Hexahedron, 20 Nodes	Voltage
SOLID123	3D	Tetrahedron, 10 Nodes	Voltage

From the aspect of total nodes, the more nodes the elements have the more time required for the simulation calculation. Hence, to reduce the calculation time, we cannot choose the SOLID122. And from the element shape, since the Tetrahedron has more accuracy than the Hexahedron, we should choose SOLID98. SOLID98 and SOLID5 has

the identical characteristics. Additionally, from the degree of freedom, we only need the Voltage and Magnetic Scalar Potential simulation and we don't need the temperature. Consequently, combined all above we finally choose the SOLID98 for the simulation of permeability and permittivity.

For both dielectric and magnetic models, element type "Solid 98" defined in ANSYS is used to construct the magnetic and dielectric inclusions, matrix and surrounding air. "Solid 98" element is tetrahedrons having 10-nodes at the corners, and 20-nodes at corners and the mid-edges, respectively. The geometries, node locations and the coordinate systems used to define a "Solid 98" element is shown in Fig 8. The output of "Solid 98" can be the data evaluated at the nodes (nodal solution) or the averages of the elements (element solution).

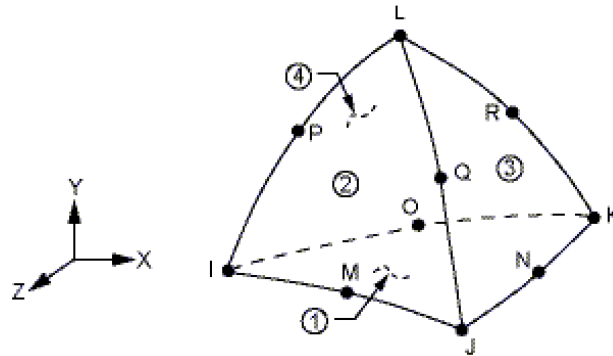


Figure 8. Diagram Showing SOLID98 Element

3.3. REV Model Construction

In the theory of composite materials, the representative elementary volume (REV) (also called the representative volume element (RVE) or the unit cell) is the smallest volume over which a measurement can be made that will yield a value representative of the whole.[59] In the case of periodic materials, one simply chooses a **periodic unit cell** (which, however, may be non-unique), but in random media, the situation is much more

complicated. For volumes smaller than the RVE, a representative property cannot be defined, and the continuum description of the material involves Statistical Volume Element (SVE) and random fields. The property of interest can include mechanical properties such as elastic moduli, hydrogeological properties, electromagnetic properties, thermal properties, and other averaged quantities that are used to describe physical systems.

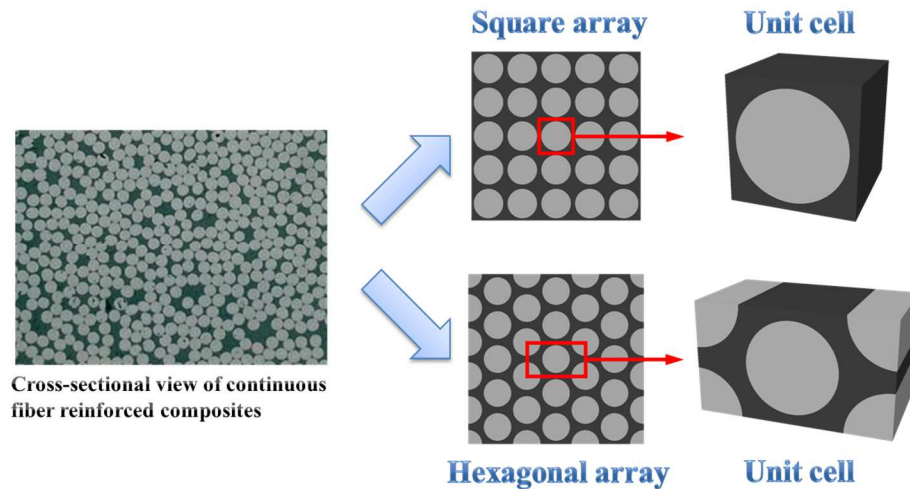


Figure 9. Schematic illustration of idealized fiber arrays and their corresponding unit cells

Form the above figure, we can see the cross-sectional view of continuous fiber dispensed in the matrix medium. The larger macroscopic real sample is break down into small microscopic array model, then, this array model has smallest group of particles in the material that constitutes the repeating pattern is the **unit cell** of the structure. The unit cell completely defines the symmetry and structure of the entire crystal lattice, which is built up by repetitive translation of the unit cell along its principal axes. The crystal structure of a material (the arrangement of fiber or nanoparticle within a given type of crystal) can be described in terms of its unit cell. The unit cell is a box containing one or more nanoparticle arranged in three dimensions.

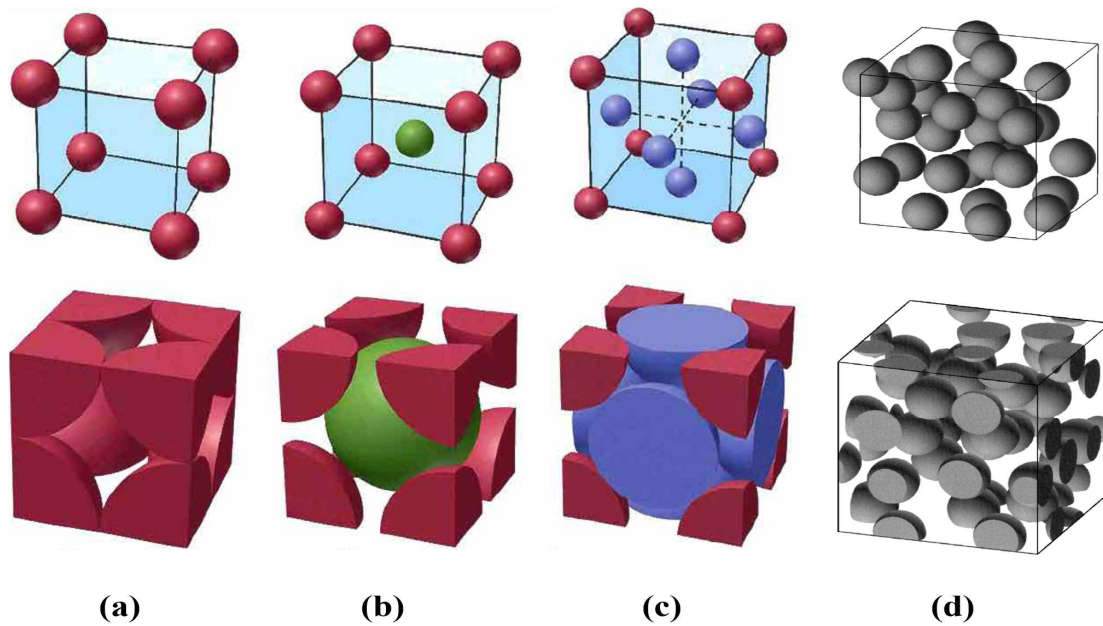


Figure 10. Cubic crystal distribution: (a) simple cubic (SC), (b) Body-Centered cubic (BCC), (c) Face-Centered Cubic (FCC), (d) Random distributed Cubic

In crystallography, the cubic (or isometric) crystal system is a crystal system where the unit cell is in the shape of a cube. Where the distribution (or arrangement) of nanoparticle is initially assumed to be simple cubic (SC), body-centered cubic (BCC), face-centered cubic (FCC), and random distributed cubic. Before meshing the model, we need to specify the geometry and properties of the materials in all regions. They include:

- (i) The fineness of the meshes;
- (ii) The structure of the inclusion arrangement (Distribution) in matrix
- (iii) The values of the linear relative permeability and permittivity of the inclusions and the matrix;
- (iv) The shape of the inclusions, which is either set to be spherical, cubic or bar respectively;
- (v) The size of the inclusions which determines their volume fraction in the composite;
- (vi) Temperature of the system is assumed as constant.

3.3.1 REV Distribution Model

In our study, initially we selected cube shape with 4 different distribution (or arrangement) of representative element volumes to conduct the Electrical Field and Magnetic Field simulation. They are Simple Cubic (SC), Body-Centered Cubic (BCC), Face-centered Cubic (FCC), and Random Distribution Models. Their geometry construction as showed below with the 8% nanoparticle volume percentage:

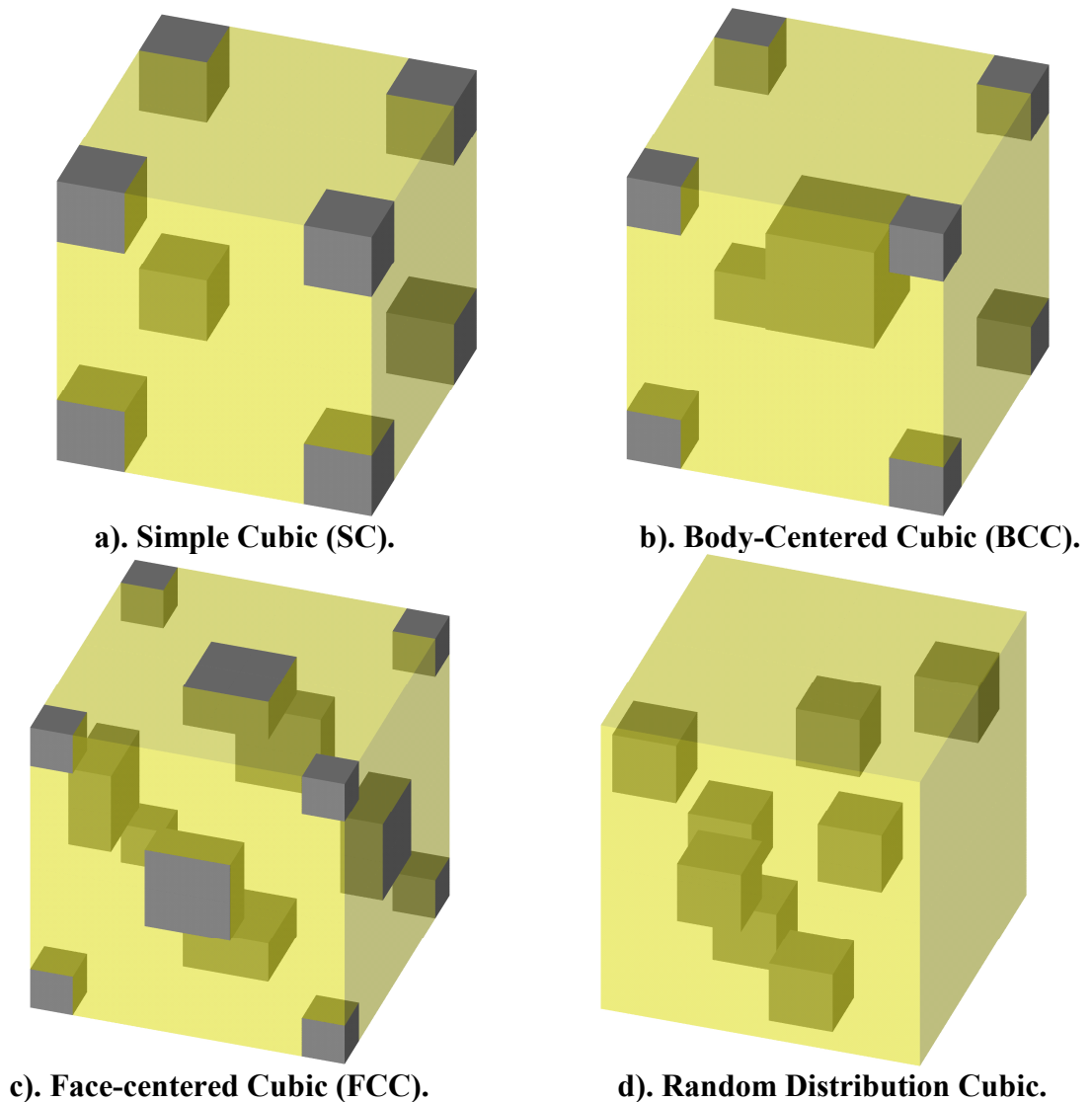
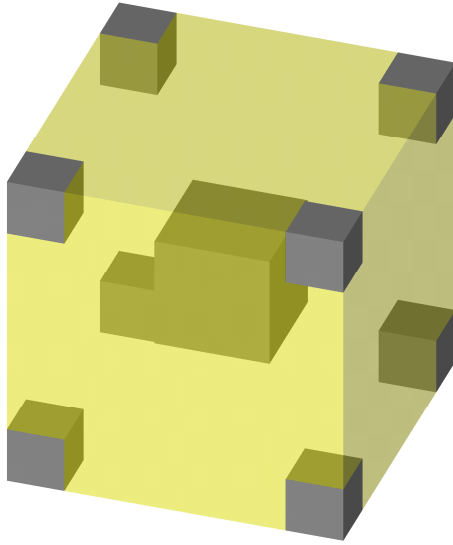


Figure 11. Geometrical Model of Distribution

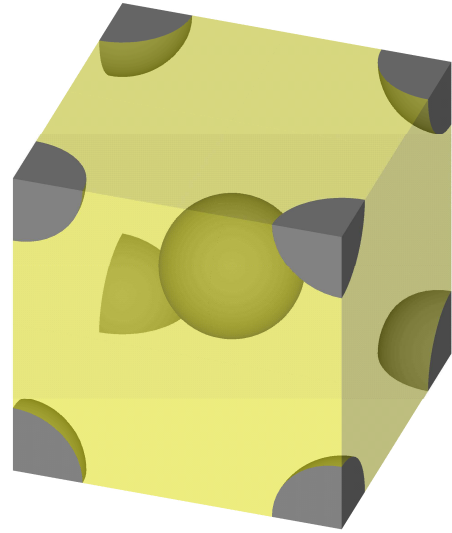
Above figure shows the geometrical model of periodic unit cell where the nanoparticle is encapsulated in the epoxy matrix. Yellow color represents the epoxy matrix, grey color represents the nanoparticle. Particularly, dark gray represents the surface of the nanoparticle and light gray represents the nanoparticle found inside the matrix. Note: all the model and result picture are captured at 8% of nanoparticle volume percentage. The volume percentage is kept constant at 8% by changing the size of nanoparticle.

3.3.2 REV Shape Model

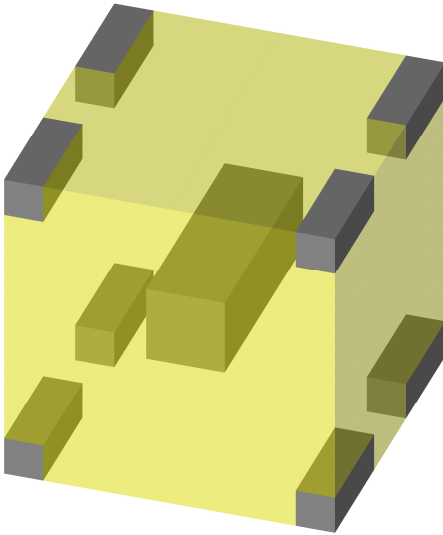
The figure 12 show the periodic unit cell with different assumption in shape of the nanoparticle encapsulated within the epoxy matrix, where the distribution (or arrangement) is considered as body-centered cubic (BCC). Three different type of shape is assumed they are cubic, spherical and bar. Bar shape as two subdivisions, one is axial directional bar and other is perpendicular directional bar represents by direction of applied field. Note: all the model and result picture are captured at 8% of nanoparticle volume percentage. The volume percentage is kept constant at 8% by changing the size of nanoparticle.



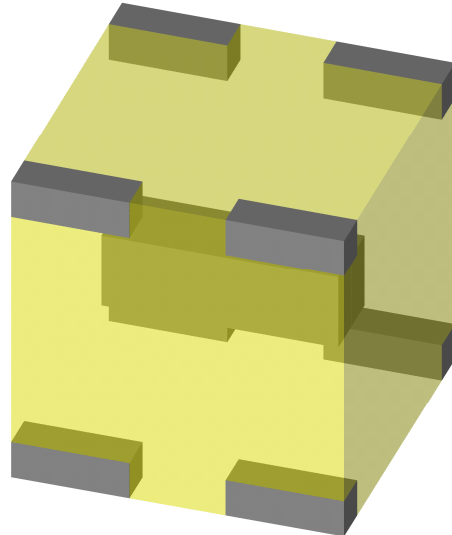
a). Cubic



b). Spherical



c).1). Axial Directional Bar



c).2). Perpendicular Directional Bar

Figure 12. Geometrical Model of Shape.

3.3.3 Monte Carlo model

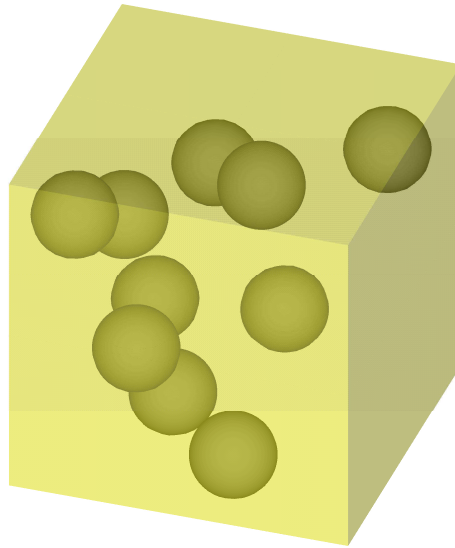


Figure 13. Monte Carlo model

When the testing specimen is viewed under the electron microscope, the nanoparticle closely looks like the spherical shape, but the real specimen having the nanoparticle randomly distributed in the epoxy matrix. Hence, for justifying the real testing specimen this periodic unit cell is designed. Having spherical shape nanoparticle randomly distributed in the epoxy matrix without intersecting each other. Note: all the model and result picture are captured at 8% of nanoparticle volume percentage. The volume percentage is kept constant at 8% by changing the size of nanoparticle.

3.4. Material Properties

Static frequency electrical and magnetic property of $\text{Ni}_{0.5}\text{Zn}_{0.5}\text{Fe}_2\text{O}_4$ nanoparticle and epoxy matrix is give as input to Ansys analysis software. Particularly, electric property such as permittivity of epoxy matrix $\epsilon_1 = 3.6$ at 60Hz frequency is noted from the reference article [60,61]. Permittivity of $\text{Ni}_{0.5}\text{Zn}_{0.5}\text{Fe}_2\text{O}_4$ nanoparticle $\epsilon_2 = 6.5$ at High frequency [62,63]. Permeability of epoxy is well known value $\mu_1 = 1$, maximum

permeability of $\text{Ni}_{0.5}\text{Zn}_{0.5}\text{Fe}_2\text{O}_4$ nanoparticle $\mu_2 = 1.889$ is derived from the article M-H curve shown below [64], and justified by other article [65]. The high saturation magnetization is likely due to the strong A-B interaction in the spinel structure. Some measured magnetic properties of $\text{Ni}_{0.5}\text{Zn}_{0.5}\text{Fe}_2\text{O}_4$ ferrite Nano powders are coercivity (HC) of 0.042 kOe, saturated magnetization (M_s) of 62.5 emu/g, and the ratio of remanence to saturated magnetization (M_r/M_s) of 0.133 [64].

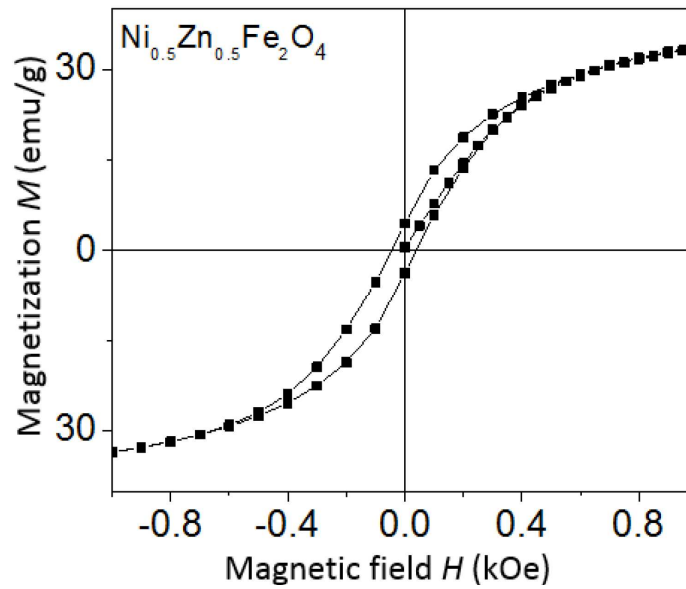


Figure 14. Magnetization curve of the synthesized $\text{Ni}_{0.5}\text{Zn}_{0.5}\text{Fe}_2\text{O}_4$ spinel ferrite Nano powder at room temperature.

B-H curve and maximum permeability $\mu_2 = 1.889$ is extracted from the above M-H curve by using formula,

$$\mu = \frac{B}{H} \quad (\text{Gaussian units}) \quad (3-1)$$

$$B = H + 4\pi M \quad (\text{Gaussian units}) \quad (3-2)$$

$$\text{Permeability, } \mu_{eff} = 1 + 4\pi \frac{dM}{dH} \quad (\text{Gaussian units}) \quad (3-3)$$

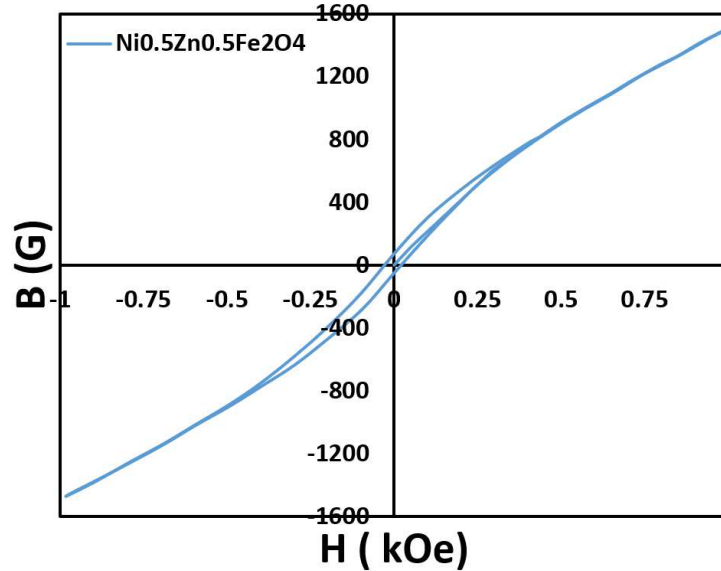
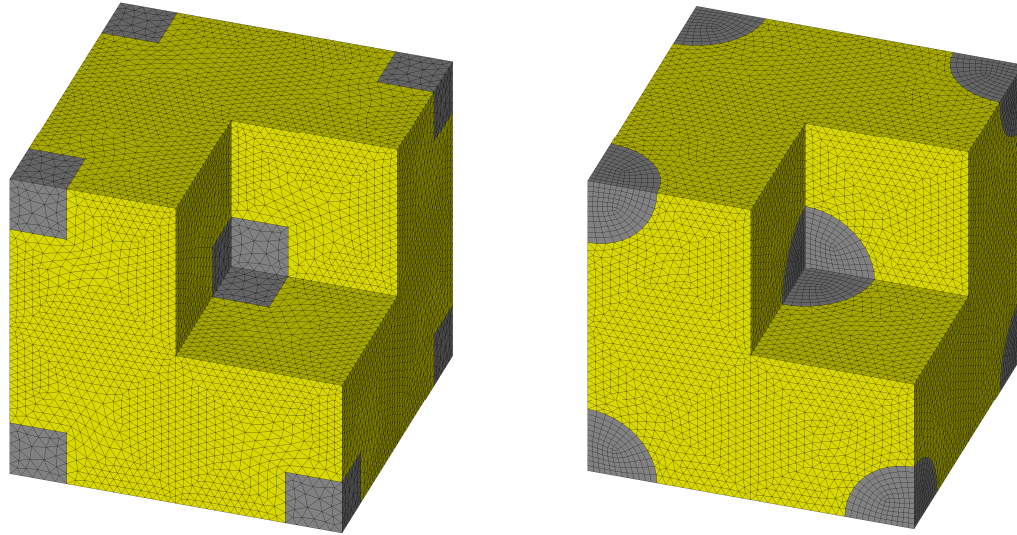


Figure 15. B-H curve of the synthesized $\text{Ni}_{0.5}\text{Zn}_{0.5}\text{Fe}_2\text{O}_4$ Nanoparticle.

3.5. REV Meshing

After fixing all these parameters, the model can be meshed with the “Smart 38Mesh” function, which helps to optimize the element sizes automatically. Alternatively, one can manually select the element size of each part. Also, the element size should be carefully selected. If it is set to be too small, the computation time would be very long, or the matrix size is too large for the computer to handle. However, if the elements are too coarse, the model would deviate from the real structure and result may not be accurate. In ANSYS software, they included 4 mesh methods: Free Meshing, Mapped Meshing, Sweep Meshing and Self-Adaption Meshing. In this application, we use Self-Adaption Meshing. During the meshing process, to keep the consistence, we define the meshing element length to be constant. The Figure.14 showed below has **Tetrahedron, 10 Nodes mesh** with the portion view and distinct color represents different material properties.



a). BCC with Cubic shape.

b). BCC with spherical shape.

Figure 16. Model Mesh

3.6. REV Boundary Condition Setup

3.6.1. Permittivity

For the simulation calculation of permittivity, we need to apply the Voltage drop between the two-opposite face of the model, which will induced the Electrical Displacement D and from the constitutive equation:

$$\mathbf{D} = \epsilon_0 \epsilon_r \mathbf{E} \quad (2-5)$$

We could derive the relative value of the permittivity ϵ_r . Since the SOLID98 is a coupling element has the 4 degrees of freedom: 3 displacement freedoms U_x , U_y , U_z and voltage V . To only have the electric relationship, we need to constraint the displacement, which defines the $U_x=0$, $U_y=0$, $U_z=0$. For example, of the Direction, we choose to apply the surface force V on the Y Direction. We applied the voltage V on the upper surface $\phi = \phi_1$ and the bottom surface $\phi = \phi_2=0$ that we could generate a uniform electrical field on the

Y Direction and keep other directions no electrical field change like the Figure.15 showed below:

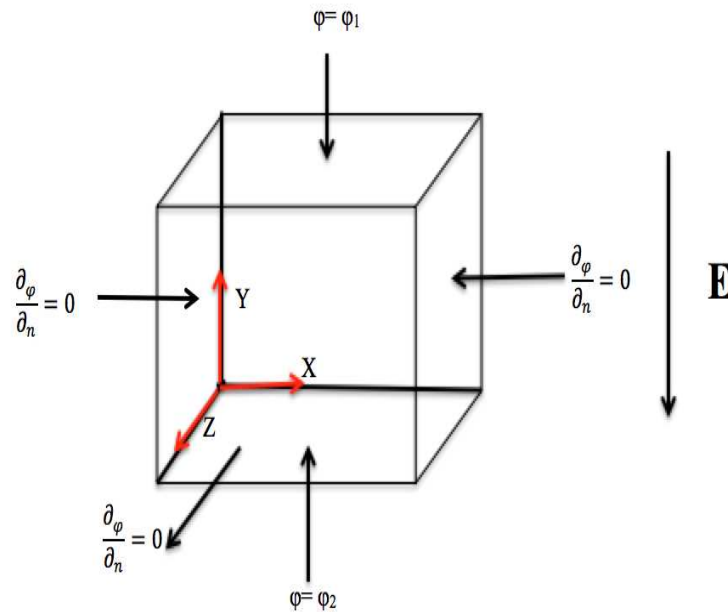


Figure 17. Boundary Condition of Permittivity Calculation

3.6.2. Permeability

For the simulation calculation of permeability, we use the similar method of calculating permittivity. We apply the surface force of Magnetic Potential, which will induce the Magnetic Flux \mathbf{B} and from the constitutive equation:

$$\mathbf{B} = \mu_0 \mu_r \mathbf{H} \quad (2-6)$$

We could derive the relative value of the permeability μ_r , like the Figure 16.

Showed below:

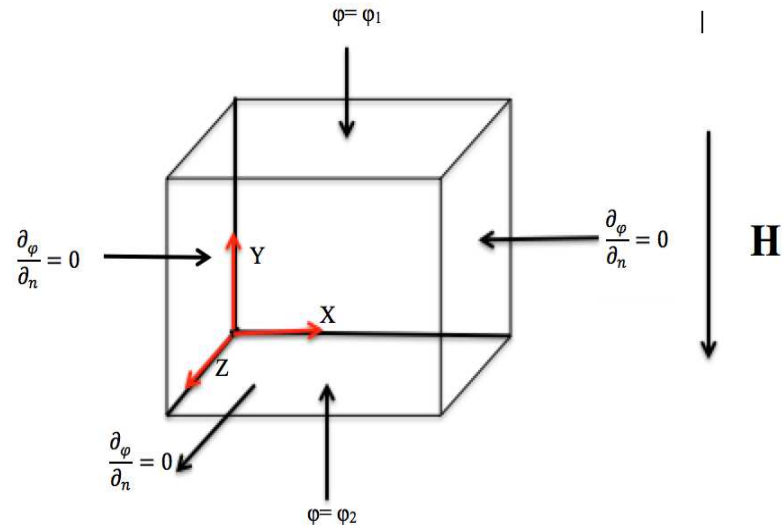


Figure 18. Boundary Condition of Permeability Calculation

The problem is then sent to the solver to get a solution. Three possible strategies are available. They are:

- (i) Reduced Scalar Potential (RSP)
- (ii) Difference Scalar Potential (DSP)
- (iii) General Scalar Potential (GSP)

For simple solution, RSP is applicable for this case.

After getting the simulated results of H , B , D , and E , which can further calculate the ϵ_{eff} and μ_{eff} of the composites like introduced earlier in Chapter 2.

$$\epsilon_{rx} = \frac{1 D_{rx}}{\epsilon_0 E_{rx}} = \frac{1 \sum_{j=1}^n D_{rij} V_j}{\epsilon_0 \sum_{j=1}^n E_{rij} V_j} \quad (2-21)$$

$$\epsilon_{eff} = \frac{\epsilon_{rx} + \epsilon_{ry} + \epsilon_{rz}}{3} \quad (2-22)$$

$$\mu_{rx} = \frac{1 B_{rx}}{\mu_0 H_{rx}} = \frac{1 \sum_{j=1}^n B_{rij} V_j}{\mu_0 \sum_{j=1}^n H_{rij} V_j} \quad (2-25)$$

$$\mu_{eff} = \frac{\mu_{rx} + \mu_{ry} + \mu_{rz}}{3} \quad (2-26)$$

$$\mu = \frac{B}{H} \quad (\text{Gaussian units}) \quad (3-1)$$

$$B = H + 4 \pi M \quad (\text{Gaussian units}) \quad (3-2)$$

$$\text{Permeability, } \mu_{eff} = 1 + 4\pi \frac{dM}{dH} \quad (\text{Gaussian units}) \quad (3-3)$$

Where, **M** is the Magnetization (emu/g) in Gaussian units.

In classical electromagnetism, **magnetization or magnetic polarization (M)** is the vector field that expresses the density of permanent or induced magnetic dipole moments in a magnetic material. The origin of the magnetic moments responsible for magnetization can be either microscopic electric currents resulting from the motion of electrons in atoms, or the spin of the electrons or the nuclei. Net magnetization results from the response of a material to an external magnetic field, together with any unbalanced magnetic dipole moments that may be inherent in the material itself. We believe that the results obtained by FEA model reflect accurately the real situation if the element sizes are properly selected.

CHAPTER 4 FABRICATION OF NANO-PARTICLE REINFORCED EPOXY BASED COMPOSITES

4.1. General Description of Fabrication Experiment Design

With the aim of optimization of EM wave ability, particles can be hosted in various parts of composites. Here, the simple case of mixing particles with polymer phase (Epoxy) is investigated and the effect of adding particles (the amount and the type) on EM wave absorption is studied. To keep the advantage of the low weight of composites over metallic parts (e.g. aluminum), the volume fraction of particles should [66] be kept as low as possible. It is proven that even a very small amount (5%) can improve the EM wave responsive ability[67]

Epon™ Resin 826 (epoxy) and Epikure W (curing agent) are two components of the epoxy resin system (matrix of nanocomposite). Based on the supplier's instructions, the weight ratio of 26.4:100 (curing agent: epoxy) is used. Also, the required amounts of epoxy/agents for a sample size (see Figure.17 bellowed) of 6cm*6cm*0.1cm (W*H*T), that gives the total volume of 3.6 cm³ for each sample is considered.



Figure 19. Final Testing Sample

For ferrite nanoparticles, which are highly reactive, extra care should be taken to avoid unwanted oxidization. A sample with approximated weight of 1g of $\text{Ni}_{0.5}\text{Zn}_{0.5}\text{Fe}_2\text{O}_4$ nanoparticles is not soluble in any kind of solution.

On a laboratory weight (precision of .0001g, which is zeroed after placing the beaker), the mixture for the nanocomposites are combined in a small glass beaker with following order:

1. The measured quantity of particles is filled in.
2. The epoxy resin would be added without delay. Mechanical stirring for 10 min at 700 rpm would continue to process.
3. Following addition of the curing agent, the mixture is mixed mechanically and ultra-sonicated for 10 min. Consequently, the mixture can be cast into the iron mold.

The iron mold is put into the oven to conclude the fabrication procedure during the baking process. For curing process, an unpressurized oven is used, that is carried out in three steps.

First, the oven is warmed up from room temperature to 80°C at a rate of $5^\circ\text{C}/\text{min}$. The pre-curing step happens at 80°C for 2 hours, followed by raising the temperature to 125°C and the post-curing step for 3 hours. Second, the samples are cooled down to room temperature and taken out of the mold. To avoid any kind of bending during the curing process and cooling period, the iron mold should be loaded with weights on the edges. Consequently, in total, ten distinct types of nanocomposites are fabricated. By using Digital Microscope, we can compare the difference of each sample.

From the fabricated sample, we could clearly see the difference of weight percentage of nanoparticle S9 ($\text{Ni}_{10.5}\text{Zn}_{0.5}\text{Fe}_2\text{O}_4$). And we could see the particle size is on the Nano-scale but due to the **aggregation of the particles**, they look like micro scale. Therefore, for next step we still need to improve the dispensation of the nanoparticles into the epoxy resin or investigate a way to grind the epoxy-based nanoparticles inclusion composite into the Nano-scale that we could have a more represented result.

4.2. Re-design Experiment Details to Get Better Constant Solution

To obtain the much more reliable result data, we need to development another way to fabricate our sample, especially in how to disperse the nanoparticles evenly in the epoxy dilute solution. As our testing sample is only a very thin film and how to fabricate a constant film with even amounts nanoparticles disperse in it becomes a crucial point for us to get the reliable result data.

After searching from some related paper and patents, we have found that the common ways to get even dispersion nanoparticles in polymer resin are usually including 2 methods: 1) Mechanical Stirring and 2) Chemical Dispersion. Generally, Chemical Dispersion could get much better constant dispersion solution than Mechanical Stirring. As Chemical Dispersion is a process by which (in the case of solids' becoming dispersed in a liquid) agglomerated particles are separated from each other and a new interface, between an inner surface of the liquid dispersion medium and the surface of the particles to be dispersed, is generated.

4.2.1. Using Coupling Agent for Nano-particles Surface Treatment

We decided to try the Chemical Dispersion method first. Due to the small diameter of the nanoparticles, large surface area, high surface energy, it is easy to agglomerate. And as the non-coordinating atoms and more nanoparticle surface, and epoxy resin combined with the likelihood of physical and chemical large, can serve to enhance interfacial bonding, and assume the role of a certain load. Therefore, in preparing to deal with nanoparticles and nanoparticle surface modification application process through adding coupling agent into particles. [68]

A coupling agent is a chemical substance capable of reacting with both the reinforcement and the resin matrix of a composite material. It may also bond inorganic fillers or fibers to organic resins to form or promote a stronger bond at the interface. May be applied from a solution or the gas phase to reinforcement, added to the resin, or both. Agent acts as interface between resin and nanoparticle (or mineral filler) to form a chemical bridge between the two. Mostly commonly used are organo trialkoxy silanes, titanates, zirconates and organic acid-chromium chloride coordination complexes.

4.2.2. Selection Specific Kind of Coupling Agent

Since our nanoparticles are nickel-zinc ferrite magnetic particles, which is similar with the patent CN 104312510 A[69]. They used KH-550 silane coupling agent ($\text{NH}_2\text{CH}_2\text{CH}_2\text{CH}_2\text{Si}(\text{OC}_2\text{H}_5)_3$) for their nickel-zinc ferrite magnetic powder. Thus, we most likely could use the same type of coupling agent for the surface treatment. After searching from the online, we found the KH-550 silane is available on several chemical products websites, like Fisher Scientific and SIGMA-ALDRICH. Based on the amount, which the patent mentioned, we do not need a lot probably 100ml or 100g will be enough.

4.2.3. The Effect of Coupling Agent on Nano-particles

To obtain the consistent solution of Epoxy Resin with Nano-particles, we used the silane-coupling agent for the surface treatment of nanoparticles. Figure.18 shows the comparison of nanoparticles ($\text{Ni}_{0.5}\text{Zn}_{0.5}\text{Fe}_2\text{O}_4$) completely reaction with coupling agent (ultrasonic dispersion for 2 hours), half reaction with coupling agent (only for mechanical stirring for 1 hour) and no reaction with coupling agent.

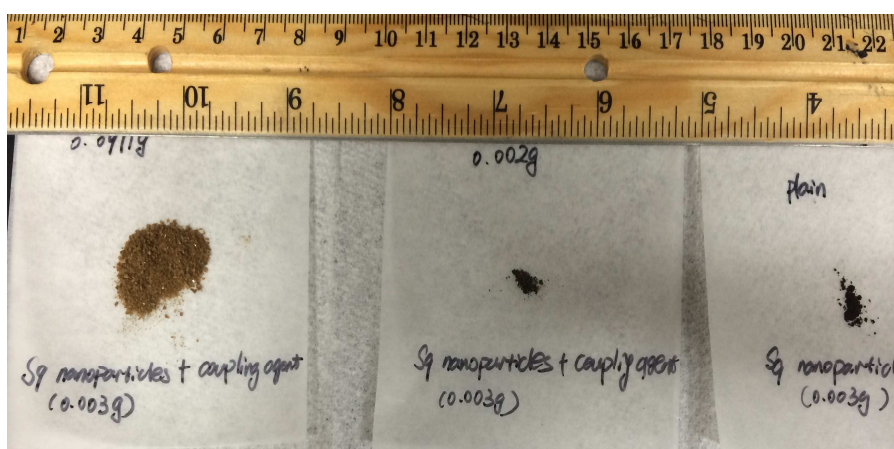


Figure 20. The Effect of Coupling Agent on Nanoparticles.

From the figure above, we could clearly see the size of these particles, for the completely reaction coupling agent the size is no longer the Nano size. But for the half reaction coupling agent the size is still much closer to Nano size. Besides, after complete reaction with coupling agent, the nanoparticles are included within coupling agent, therefore the weight of the nanoparticles 0.0971g increased incrementally compared with the original weight 0.003g. From here, we think 2% of coupling agent might be a bit over for those particles. Next time we would like to decrease down to 0.5%.

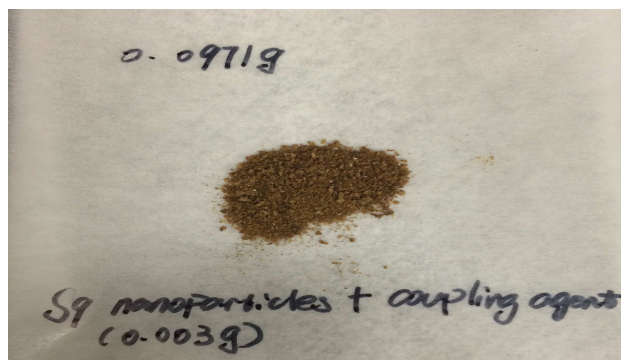


Figure 21. The Morphology of Nano-particles after Reaction with Coupling Agent.

Although, from the solution with Epoxy with Nano-particles, we could clearly tell that the completely reaction one is emulsion system which reach our goals to get the better dispersion of the nanoparticles into epoxy resin. But the half reaction one could still easily to tell the solvent and solute even the size could be much smaller than the completely reaction one. So, adding the coupling agent would be good idea for the better dispersion of nanoparticles into epoxy resin.

After with spin coater, in which we set the spin speed is 500 rpm with 40 second, we got the film coating on our substrate.

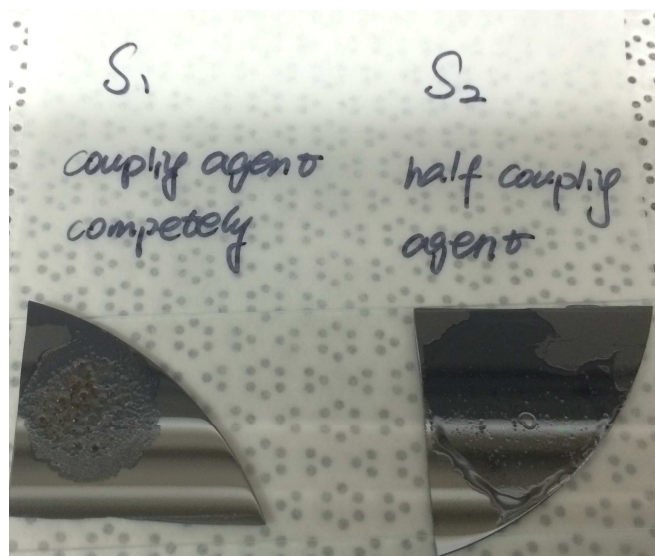


Figure 22. The Comparison of Coupling Agent Reaction Time.

From the picture above, we could conclude that using the coupling agent we are able to get the consistent nanoparticle reinforced epoxy-based film, but the only concern is we need the Nano grinding machine to further obtain the Nano-size particles otherwise the particles we got directly from the coupling agent reaction will be too big to be used as nanoparticles, which will affect our coating.

Therefore, from this process, we need to avoid the mechanical stirring since the magnetic stirrer would absorb all the nanoparticles onto itself through the magnetism. Hence, we suggest only use ultrasonic dispersion would be a good way to disperse the nanoparticles.

The amount of the coupling agent (2% of ethanol) would too much for the nanoparticles; We need to narrow down the ration of ethanol with coupling agent maybe to 0.5% next time. After the nanoparticles completely reaction with coupling agent, we would have need the further Nano grinding as the particles we got from reaction is no longer Nano-size. Once we could have the Nano-grinding machine, we could be able to fabricate abundant nanoparticles at one time. Through this way, we could be able to get ideal size nanoparticles and disperse evenly in Epoxy Resin.

4.2.4. Steps for Re-Designed Experiment

First of all, added ethanol and a coupling agent and nanoparticles together for mechanical stirring for at least 60min, and then ultrasonic dispersing at least 60min, wherein the quality coupling agent 1% -3% by mass of ethanol, said coupling agent is a silane coupling agent, aluminum acid esters coupling agents, coupling agents or aluminum zirconium esters titanate coupling agents. Secondly, take a dilute epoxy resin solution with

acetone and preheated at 60-70 ° C conditions 20-30min, step 1) was modified nanoparticles are added to the preheated epoxy resin, epoxy resin and then again adding hardener mechanical stirring for at least 60min, and then ultrasonic dispersion at least 60min, and finally vacuum degassing 20~60 minutes, wherein the epoxy resin, nanoparticles, a coupling agent and a curing agent of the four-mass ratio of 100: (Γ5): (0.0Γ0.15): (3 (Γ50)). Finally, we fabricated the well dispensed nanoparticle in epoxy matrix, unlike the figure 18,19,20.

4.3. Testing Result

As the fabrication method introduced above, we use the epoxy as the matrix and add $\text{Ni}_{0.5}\text{Zn}_{0.5}\text{Fe}_2\text{O}_4$ nanoparticles with different weight ratio (0.1%, 0.3% and 0.6%) for the comparison.

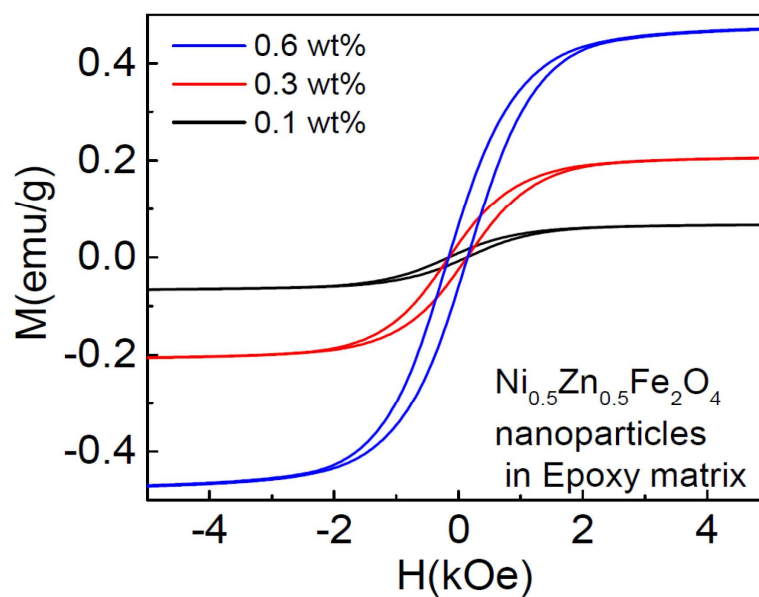


Figure 23. Magnetization curve of the synthesized epoxy matrix nanocomposites at room temperature.

The isothermal magnetization curves $M(H)$ of the nanocomposite samples with various weight fractions of the $\text{Ni}_{0.5}\text{Zn}_{0.5}\text{Fe}_2\text{O}_4$ nanoparticles were measured using VersaLab Vibrating Sample Magnetometer (VSM) at room temperature ($T = 300 \text{ K}$), as shown in Fig. 26. The measurements were used to validate the modeling results. Note: M -stands for Magnetization and H -stands for Magnetic Field. Units notified here CGS or Electromagnetic unit.

From the M - H curve we can derive the permeability (μ_{eff}) by using the slope of the curve at every point and using the equation (3.3). Figure 27 shows the permeability μ_{eff} (no unit) vs magnetic field H (kOe).

$$\text{Permeability, } \mu_{\text{eff}} = 1 + 4\pi \frac{dM}{dH} \quad (\text{Gaussian units}) \quad (3-3)$$

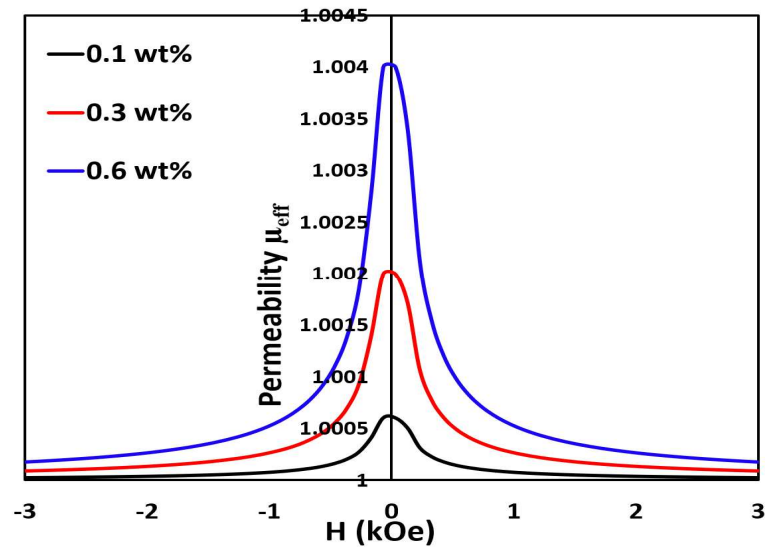


Figure 24. Permeability μ_{eff} curve of the synthesized epoxy matrix nanocomposites at room temperature.

There are three types of permeability, initial permeability, complex permeability and maximum permeability. Entire research is concentrated on the maximum permeability, which is derived from the M - H curve of experimental result obtained from vibrating sample magnetometer. Note: Unit used here is CGS or Electromagnetic unit.

Table 2. Experimental data.

Weight percentage (%)	Coercivity, H_c (Oe)	Remanent magnetization, M_r (emu/g)	Saturation Magnetization, M_s (emu/g)	Maximum Permeability, μ_{max}
0.1	160	0.0005	0.06	1.0006
0.3	159	0.0025	0.2	1.002
0.6	157	0.083	0.4	1.004

From the VSM experimental result, it is clear that increases in percentage of $Ni_{0.5}Zn_{0.5}Fe_2O_4$ nanoparticles adding to the epoxy resin, affects the electromagnetic property. Where saturation magnetization M_s and effective maximum permeability μ_{eff} increase by increase the percentage of $Ni_{0.5}Zn_{0.5}Fe_2O_4$ nanoparticles. Consequently, in order to attain a desired permeability possessed nanocomposites, we could vary the percentage of nanoparticles encapsulated in epoxy matrix.

CHAPTER 5 RESULT DISCUSSION

5.1 Modeling Result

The essential step before conducting computer modeling of the nanocomposites was the construction of a solid model and the assumption of the initial conditions. In this work, a three-dimensional model on magnetic and dielectric properties of two-phase mixture (epoxy polymer matrix and $\text{Ni}_{0.5}\text{Zn}_{0.5}\text{Fe}_2\text{O}_4$ ferrite magnetic nanoparticles) was constructed. We simulated different geometric models with the nanoparticles inclusive in the polymeric matrix increased from 50% to 0.1% and applied both electrical and magnetic fields in X, Y and Z directions respectively to get the effective permittivity and permeability of our designed composites.

5.1.1. Periodic Model

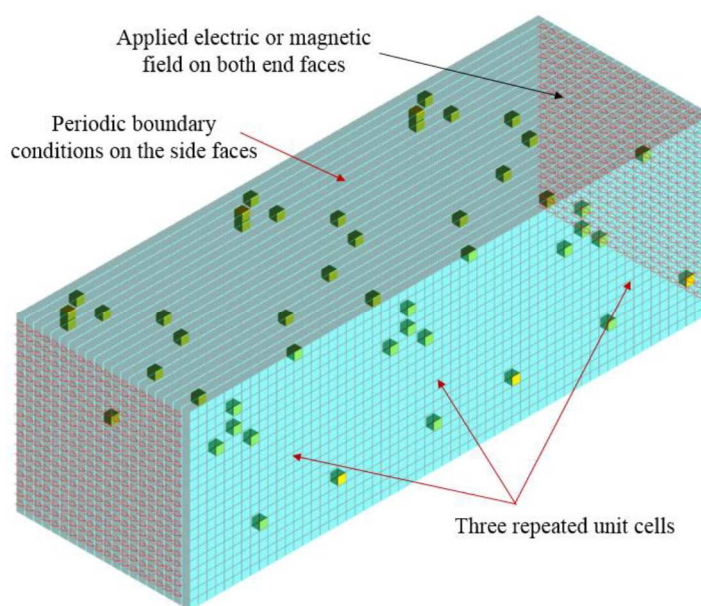


Figure 25. Periodic boundary condition model.

This model was consisted of Three-unit cell periodically arranged in z-axis, and other two direction x,y-axis are given as periodic boundary condition. In the unit cell, the

nanoparticles were distributed based on Monte Carol method, as shown in Fig. 28. An electric or magnetic field on both end faces was applied.

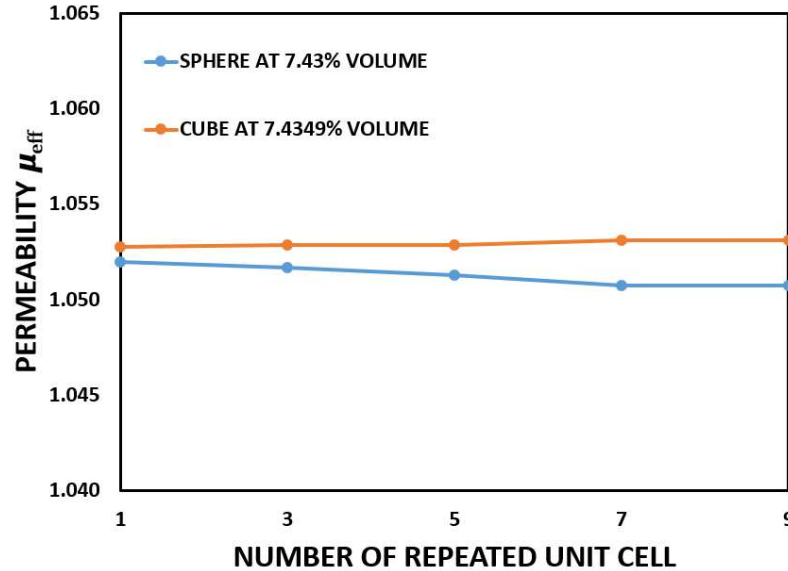


Figure 26. Repeated unit cell graph.

Similarly, number of repeated unit cell used is tested based on output material property of composite, here permeability of material is taken into account. From the graph figure.29 shows constant result even when we increase the repeated number of unit cell. Both the cube and sphere shape of nanoparticle is simulated at different volume percentage. There is slight variation in trend, we doubted that it may be because of element size used in simulation. So, we came to perception that number of repeated unit cell does affect the modelling result.

5.1.2. Element Size Convergence Study

We try to sort out the number of unit cell problem, with the element size. Here, the number of element used for the simulation is considered. We simulate constant 8% volume

percentage of nanoparticle by varying the different element size and different repetitive unit cell. Output result such as permeability and solution time is extracted.

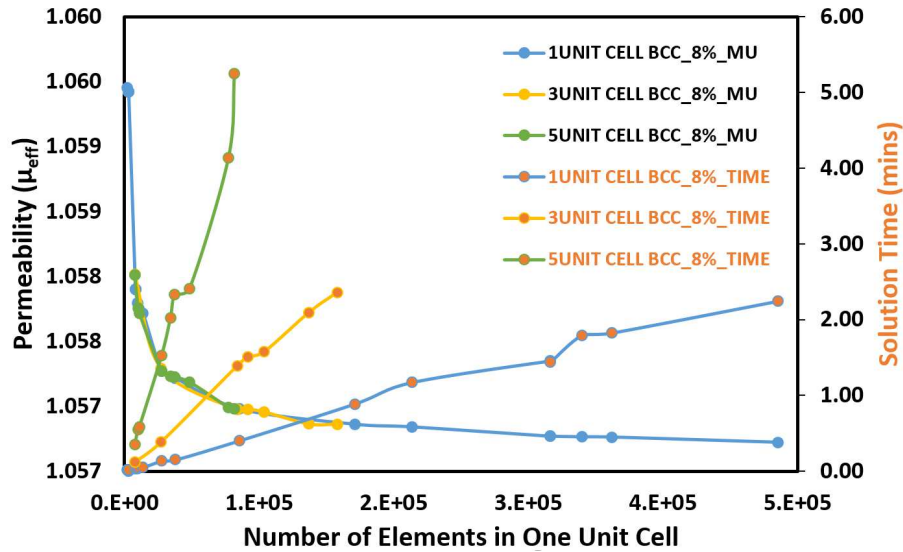
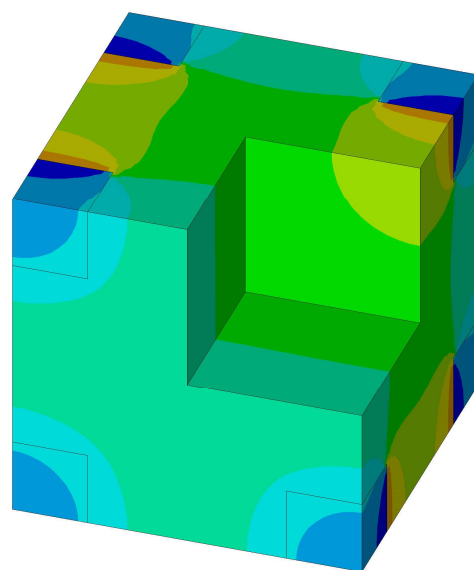


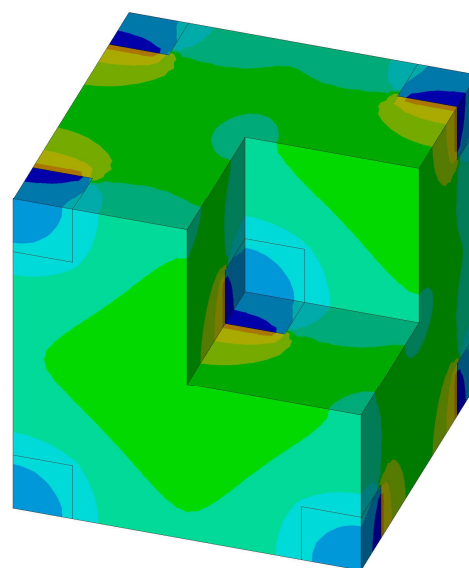
Figure 27. Element size convergence graph.

From the above graph, it is clear that element size plays major role in simulation. In ansys, as per academic version software, we can use only limited number of elements for the simulation. 5 and 3 repetitive unit cell need more element plus element size will be coarse, but in 1 unit cell simulation we can use the maximum number of element and that size of the element is very fine enough to converge and give accurate result. On the other hand, solution time is also the critical parameter in simulation, eventhough we use more element for 1 unit cell model, solution is considerably smaller than other. So, it is clear that 1 repetitive unit cell is more than enough to converge to the accurate result, then our remaining model is simulated with 1 unit cell with maximum element and fine element size.

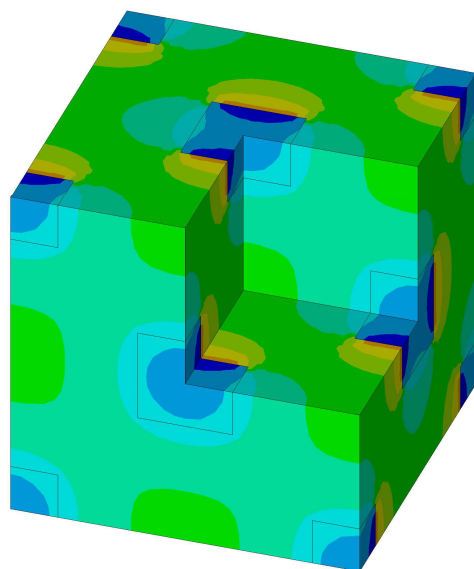
5.1.3. Effects of Nanoparticle Distribution



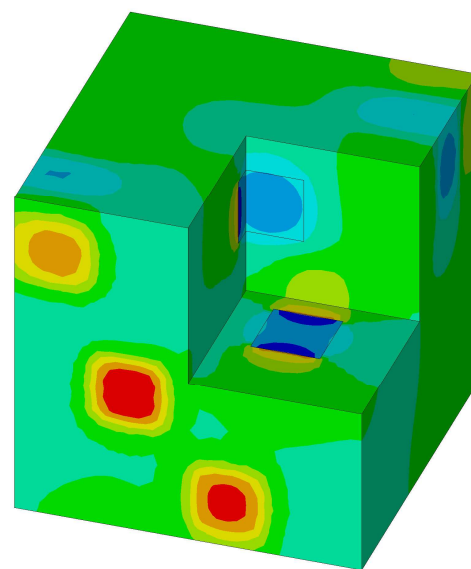
(a) SC



(b) BCC



(c) FCC



(d) Random

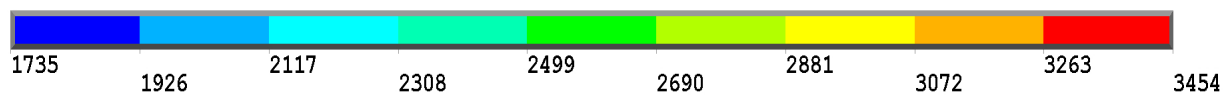
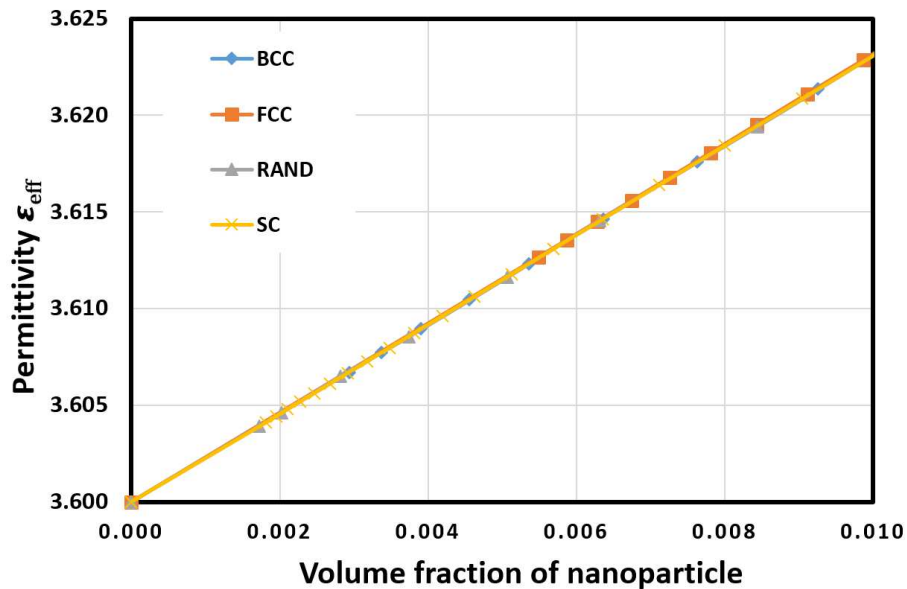
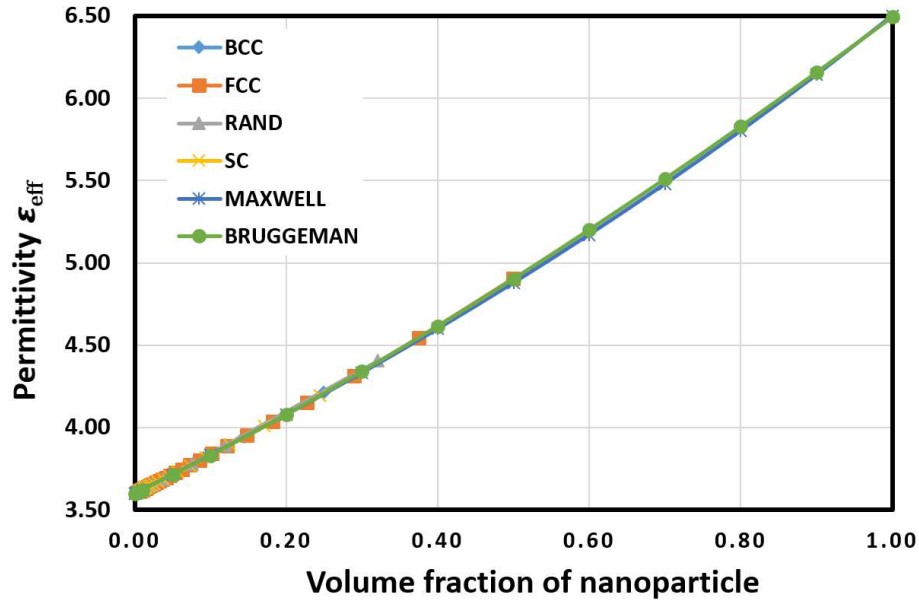


Figure 28. Electric field distribution (V/cm) for various cubic nanoparticle distributions of 8 vol% nanoparticles.

After fixing the element size problem, 1 unit cell model is considered to simulate the effects of $\text{Ni}_{0.5}\text{Zn}_{0.5}\text{Fe}_2\text{O}_4$ ferrite magnetic nanoparticles. Figure 31, shows the contour map of portioned unit cell, where portion is used to visualize the interaction between the particle. Here, for example electric field (V/cm) distribution for various cubic nanoparticle arrangement (distribution) of constant 8% volume of nanoparticle such as simple cubic (SC), body-centered cubic (BCC), face-centered cubic (FCC) and random distributed unit cell is displayed. By visual inspection of different distributed model, we can just guess that interaction between nanoparticle is strong or weak. In simple cubic electric field distribution, we can come to small deduction that the distance between the nanoparticle are smaller than other three distribution. Because, nanoparticle size is varied in constant one unit cell cubic size. Also we used the period boundary condition, the interaction between the next unit cell is also considered.



(a)

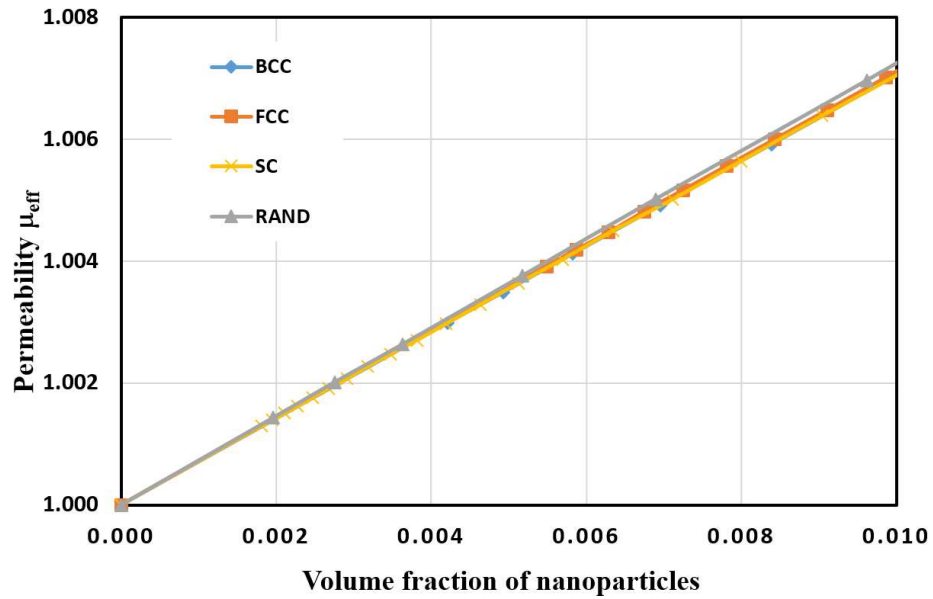


(b)

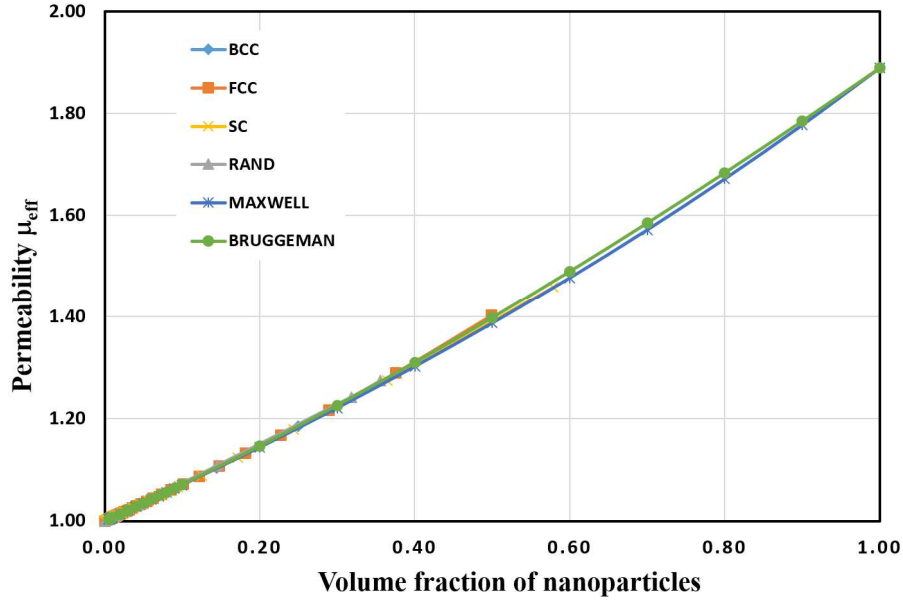
Figure 29. Permittivity vs. volume fraction of nanoparticles for various distributions and comparing with analytical calculations. Volume fraction ranging 0~1% (a) and 0~100% (b).

Permittivity is calculated by equation (2.19 to 2.22) where, electric field intensity (E) and electric displacement (D) data is extracted from the simulation. Figure 32(a) shows permittivity vs. volume fraction of nanoparticles for various distributions such as simple cubic (SC), body-centered cubic (BCC), face-centered cubic (FCC) and random distributed in volume fraction ranging form 0-1%, it is clear that these four distributions have same permittivity value over the all amount of $\text{Ni}_{0.5}\text{Zn}_{0.5}\text{Fe}_2\text{O}_4$ ferrite magnetic nanoparticles. Figure 32(b) use the Maxwell and Bruggeman equation (2.27,2.29) to compare the distribution result and to justify the simulation value by analytical method, percentage of $\text{Ni}_{0.5}\text{Zn}_{0.5}\text{Fe}_2\text{O}_4$ ferrite magnetic nanoparticles in scale of 0-100% in exactly match the simulation and analytical result, so the simulation data is verified. Then we can conclude that if, $\text{Ni}_{0.5}\text{Zn}_{0.5}\text{Fe}_2\text{O}_4$ nanoparticle distribution in epoxy matrix does not alter the permittivity of the composite.

Similarly, as like figure 31 magnetic field density and magnetic flux density contour map of portioned unit cell is obtained. Magnetic field (Oe) distribution for various cubic nanoparticle arrangement (distribution) of constant 8% volume of nanoparticle such as simple cubic (SC), body-centered cubic (BCC), face-centered cubic (FCC) and random distributed unit cell is displayed.



(a)

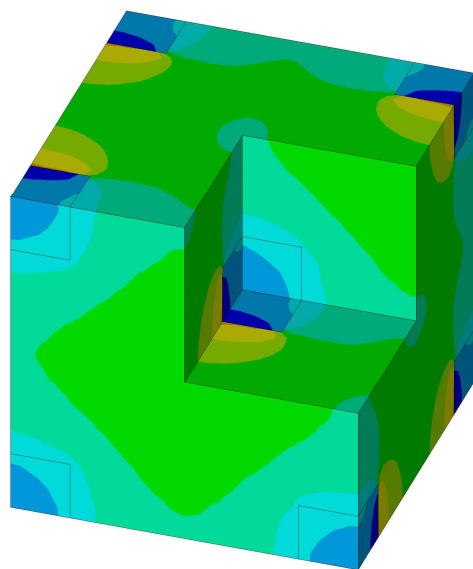


(b)

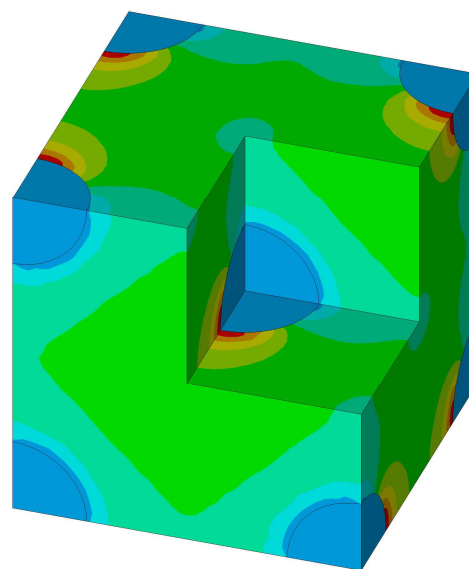
Figure 30. Permeability vs. volume fraction of nanoparticles for various distributions and comparing with analytical calculations. Volume fraction ranging 0~1% (a) and 0~100% (b).

Similarly, permeability is calculated by equation (2.23 to 2.26) where, Magnetic field density (H) and magnetic flux density (B) data is extracted from the simulation. Figure 33(a) shows permeability vs. volume fraction of nanoparticles for various distributions such as simple cubic (SC), body-centered cubic (BCC), face-centered cubic (FCC) and random distributed in volume fraction ranging from 0-1%, it is clear that these four distributions have same permeability value over the all amount of $\text{Ni}_{0.5}\text{Zn}_{0.5}\text{Fe}_2\text{O}_4$ ferrite magnetic nanoparticles. Figure 33(b) use the Maxwell and Bruggeman equation (2.28,2.30) to compare the distribution result and to justify the simulation value by analytical method, percentage of $\text{Ni}_{0.5}\text{Zn}_{0.5}\text{Fe}_2\text{O}_4$ ferrite magnetic nanoparticles in scale of 0-100% in exactly match the simulation and analytical result, so the simulation data is verified. Then we can conclude that if, $\text{Ni}_{0.5}\text{Zn}_{0.5}\text{Fe}_2\text{O}_4$ nanoparticle distribution in epoxy matrix does not alter the permeability of the composite.

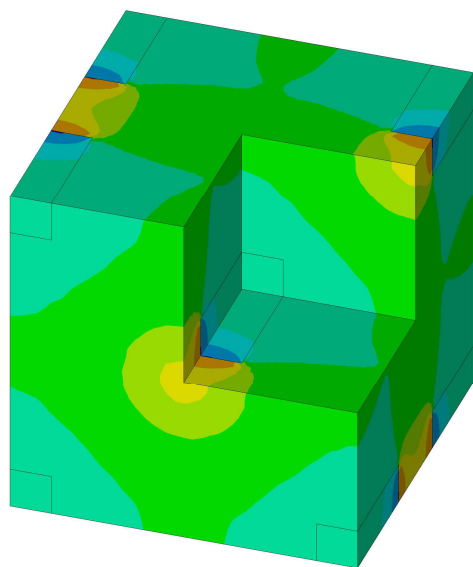
5.1.4. Effects of Nanoparticle shape



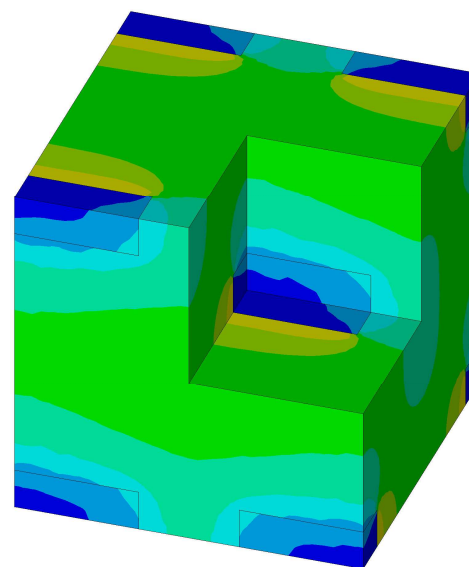
(a) Cube



(b) Sphere



(c).1). Axial Directional Bar



(c).2). Perpendicular Directional Bar

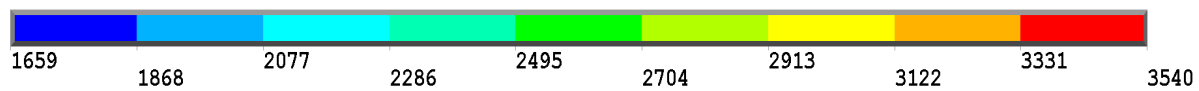


Figure 31. Magnetic field distribution (Oe) for various particle shapes with BCC distribution.

Shape of $\text{Ni}_{0.5}\text{Zn}_{0.5}\text{Fe}_2\text{O}_4$ ferrite magnetic nanoparticles and their effects in material properties were studied. For example, figure 34 shows the magnetic field density (Oe) contour map of portioned unit cell. Magnetic field (Oe) distribution for various shape of nanoparticle at constant BCC and constant 8% volume of nanoparticle are plotted. Shape such as cube, sphere, axial directional bar and perpendicular directional bar unit cell is displayed. By visual inspection of magnetic field distribution, there is something suspicious.

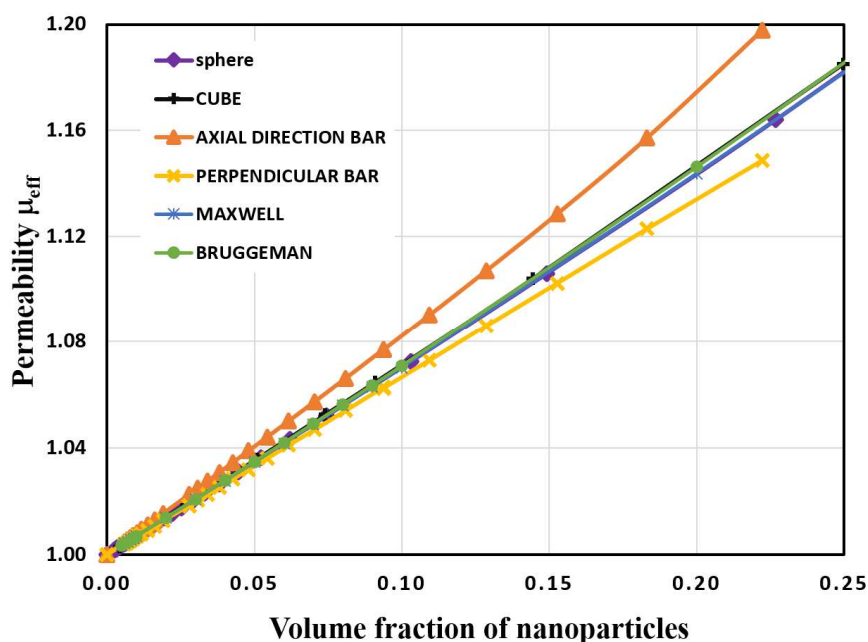


Figure 32. Permeability vs. volume fraction of nanoparticles for various shape and comparing with analytical calculations.

Similarly, permeability is calculated by equation (2.23 to 2.26) where, Magnetic field density (H) and magnetic flux density (B) data is extracted from the simulation. Figure 35 shows permeability vs. volume fraction of nanoparticles for various shape. The graph clears our suspicious doubt, spherical and cube shape of $\text{Ni}_{0.5}\text{Zn}_{0.5}\text{Fe}_2\text{O}_4$ ferrite magnetic nanoparticles match exactly as analytical calculation (Maxwell and Bruggeman) because, Maxwell and Bruggeman consider spherical inclusion as their nanoparticle shape, but even

cube shape gives same result because in figure 34 cube shape formed as spherical magnetic field. On the other hand, material property shows great variation between bar shape, axial directional bar gives higher permeability and permittivity than other shape. Perpendicular directional bar gives lower permeability and permittivity than spherical and cube shape, lot of literature support this result. Axial direction bar means direction perpendicular to electromagnetic wave propagation. As in figure 1 show electromagnetic wave propagate direction perpendicular to both magnetic and electric field, hence in axial directional bar model electromagnetic wave propagate in perpendicular direction. Morihiko Matsumoto and Yoshimori Miyata [33] designed a soft magnetic material with flaky thin amorphous metal particles about 2 μm thick and that are aligned in polymer in the direction perpendicular to electromagnetic wave propagation. They have stated that material yields a permeability two to three times higher than the spinel-type ferrite system in the quasi-microwave band. Similarly, as in literature [34]. Our result also gives the same result at stated by literature.

5.1.5. Monte Carlo Model Result

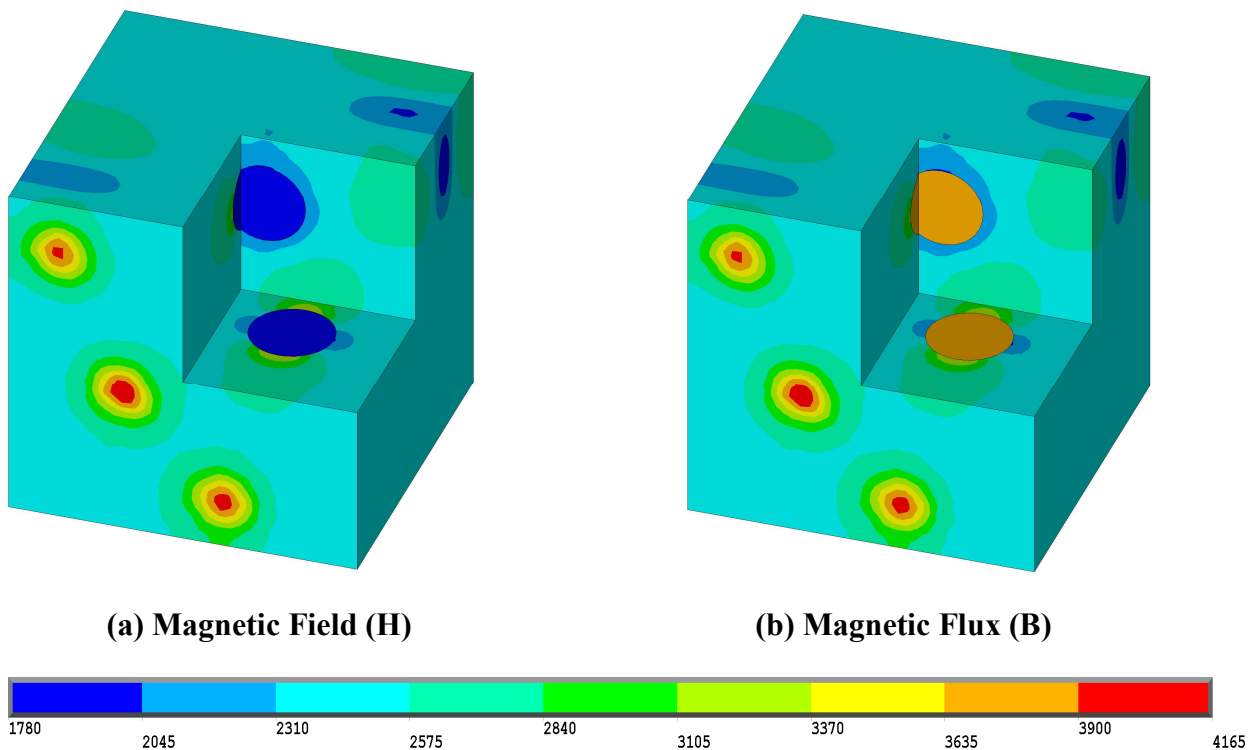


Figure 33. Magnetic field and Magnetic flux of Monte Carlo model.

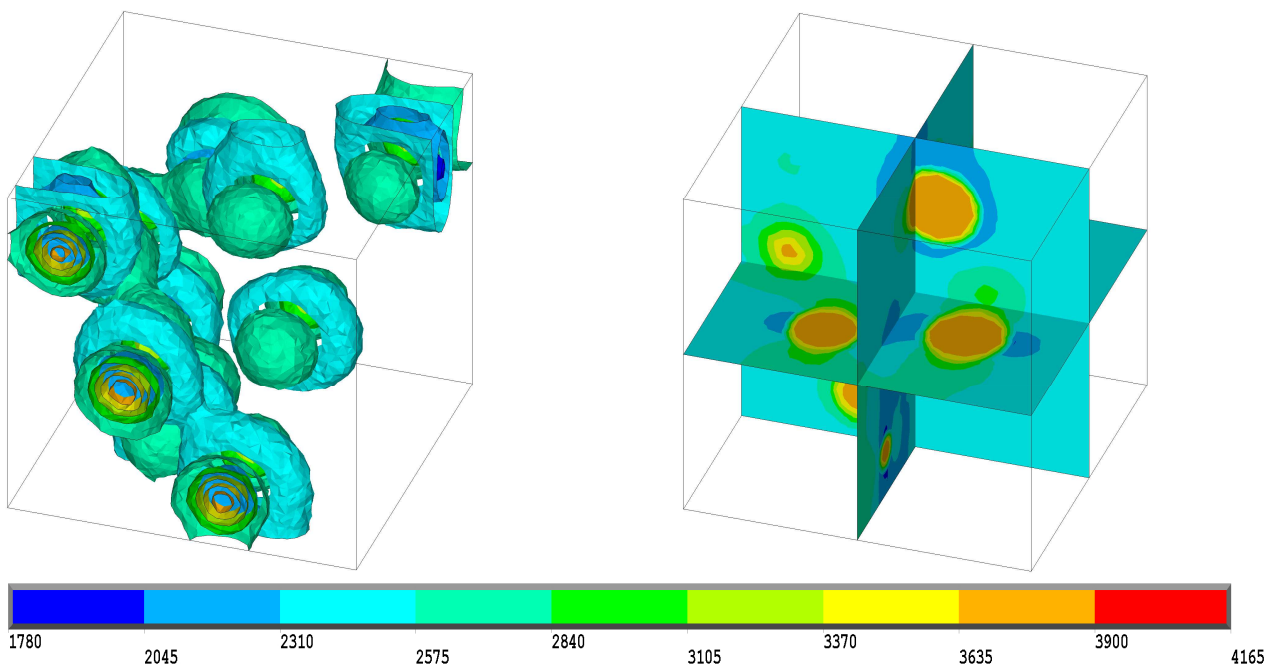


Figure 34. Magnetic field (Oe) interaction in Monte Carlo model.

This Monte Carlo model is built to match the exact specimen and to see their interaction between the $\text{Ni}_{0.5}\text{Zn}_{0.5}\text{Fe}_2\text{O}_4$ ferrite magnetic nanoparticles in epoxy matrix. Figure 36 show the portion unit cell of magnetic field density (Oe) and magnetic flux density (Gauss), where nanoparticle is arranged randomly by Monte Carlo method. Both contour of magnetic field and magnetic flux looks similar and produce similar magnetic field and flux outside the nanoparticle but, inside the nanoparticle, magnetic field is least value then surrounding and magnetic flux has higher value. Figure 37 is displayed to show the interaction between the nanoparticle, here we can see the influence of one magnetic particle on other. One thing we can see that one particle produce magnetic field which affect the other particle only on the surface of the nanoparticle, it does not affect inner solid of nanoparticle. Monte Carlo model give same permeability and permittivity as the random cube distribution, also match with the analytical result.

5.2. Validation

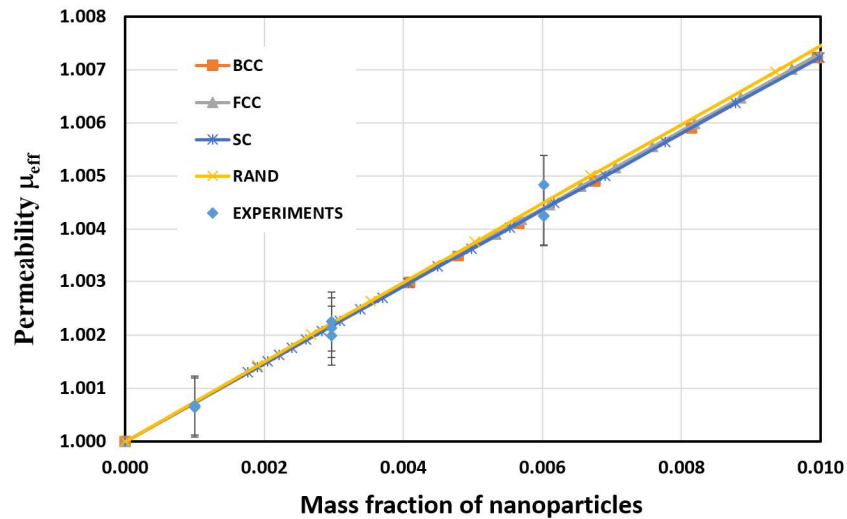


Figure 35. Comparison of modeling with experiments for permeability vs. mass fraction of nanoparticles.

In scientific engineering, validation is point of proofing that simulated result is true and accurate to the real experimental result with some error value. Figure 38 shows the comparison of modeling (simulated) result with the experimental result, here simulated permeability and experimental permeability is plotted vs mass fraction of nanoparticle. Simulation result are in volume percentage of nanoparticle, but experiment data are in mass percentage of nanoparticle, we use the real density of nanoparticle to convert volume percentage to mass percentage.

$$m_{fnp} = \frac{V_{fnp} * \rho_{np}}{(V_{fnp} * \rho_{np}) + (V_{fm} * \rho_m)} \quad (5-1)$$

Where, m_{fnp} – mass fraction of nanoparticle.

V_{fnp} , V_{fm} – volume fraction of nanoparticle and matrix.

ρ_{np} , ρ_m – density of nanoparticle and matrix.

Density of matrix is 1.194 g/cm³, density of Ni_{0.5}Zn_{0.5}Fe₂O₄ ferrite magnetic nanoparticles we used for entire research is 1.159 g/cm³.

In figure 38, simulation result of effective permeability μ_{eff} of simple cubic (SC), body-centered cubic (BCC), face-centered cubic (FCC) and random distributed exactly trace the same path as experimental result having least 0.001% error, we already proved that simulation and analytical result match each other. Here we can come to small deduction that distribution of nanoparticle does not influence the material property such as permittivity and permeability.

Table 3. Validation of simulation result with experimental data.

Mass percentage (%)	Experimental Saturation magnetization (emu/g)	Calculated Saturation magnetization (emu/g)	Mean value of simulated permeability μ_{eff}	Mean value of experimental permeability μ_{eff}	Error of permeability μ_{eff} (%)
100	62.5	62.5	1.889	1.889	0
0.6	0.4	0.375	1.004452	1.004448	3.91e-4
0.3	0.2	0.1875	1.002264	1.002123	0.014
0.1	0.06	0.0625	1.0007303	1.000661	0.0069
0	0	0	1	1	0

Above table 3 is tabulated to show the error percentage of simulation vs experimental result. First saturation magnetization of composite is calculated by formula.

$$\mathbf{M_{s \text{ calculated}} = M_{s100\%np} \times m_{fnp}} \quad \mathbf{(5-2)}$$

Saturation magnetization is liner with the mass fraction of nanoparticle (m_{fnp}). Where, saturation magnetization of 100% $\text{Ni}_{0.5}\text{Zn}_{0.5}\text{Fe}_2\text{O}_4$ ferrite magnetic nanoparticles multiply by mass fraction of nanoparticle give the calculated saturation magnetization of composite at required mass fraction.

Experiment saturation magnetization and calculated magnetization are nearly equal. In contrast, mean value of simulated permeability means average of all model such as simple cubic (SC), body-centered cubic (BCC), face-centered cubic (FCC) and random

distributed model result is tabulated against the mean value of experimental result. The error value is calculated by formula.

$$\mathbf{error\ \% = \left(\frac{experimental-simulated}{experimental} \right) X\ 100} \quad (5-3)$$

Relative error percentage is fair enough to justify the simulation result is accurate.

5.3. Conclusion

The epoxy polymer matrix nanocomposites were fabricated by dispersing the spinel structured nickel zinc ferrite ($\text{Ni}_{0.5}\text{Zn}_{0.5}\text{Fe}_2\text{O}_4$) nanoparticles through ultrasonic agitation mixing for developing magnetic responsive material. A three-dimensional finite element analysis model was developed for modeling the magnetic and dielectric properties of the nanocomposites. The composites' effective permittivity and permeability were extracted from the modeling data. The effects of the ferrite nanoparticle's concentration, shape, and distribution on the effective permittivity and permeability of the nanocomposites were systematically investigated by computer modeling. No significant effect of the ferrite nanoparticle's distributions (body-centered cubic, face-centered cubic, simple cubic and random distributions) was found on the permittivity and permeability of the nanocomposites

But, alternatively the permeability and permittivity vary with the mass fraction and shape of the $\text{Ni}_{0.5}\text{Zn}_{0.5}\text{Fe}_2\text{O}_4$ ferrite magnetic nanoparticles encapsulated in epoxy resin. Especially, spherical and cube shape of $\text{Ni}_{0.5}\text{Zn}_{0.5}\text{Fe}_2\text{O}_4$ ferrite magnetic nanoparticles match exactly as analytical calculation (Maxwell and Bruggeman) because, Maxwell and Bruggeman consider spherical inclusion as their nanoparticle shape. In contrast, material property shows great variation between bar shape, axial directional bar gives higher

permeability and permittivity than other shapes. Perpendicular directional bars give lower permeability and permittivity than spherical and cube shapes. So, the appropriate material property is achieved by selecting the proper amount of $\text{Ni}_{0.5}\text{Zn}_{0.5}\text{Fe}_2\text{O}_4$ ferrite magnetic nanoparticles added to the epoxy resin and the shape of $\text{Ni}_{0.5}\text{Zn}_{0.5}\text{Fe}_2\text{O}_4$ ferrite magnetic nanoparticles is also to be selected to get the required permeability and permittivity.

The appropriate combination of permeability and permittivity properties is selected based on the shape and percentage of nanoparticle for the synthesis of Radar (or Radiation) Absorbent Material (RAM) providing wide-ranging bandwidth.

CHAPTER 6 FUTURE WORK

To select good RAM composite, appropriate shape and mass fraction of $\text{Ni}_{0.5}\text{Zn}_{0.5}\text{Fe}_2\text{O}_4$ ferrite magnetic nanoparticles is added to epoxy resin respectively to get higher band-width providing composite material. Now, we have different value of permeability and permittivity from the FEA approach. These values are input to the solid block and their scattering parameter s_{11} (or reflection loss) is analyzed.

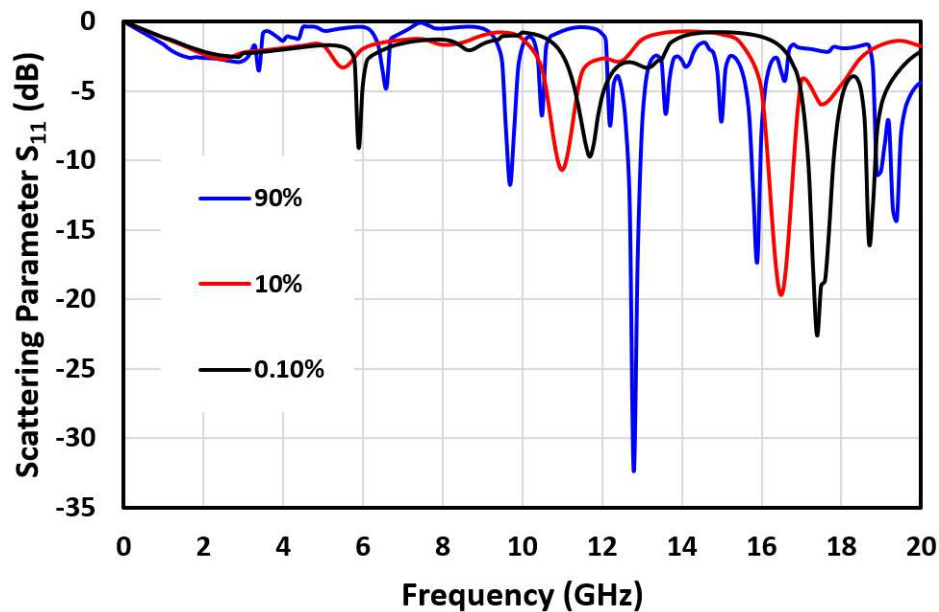


Figure 36. Scattering parameter vs. Frequency.

As explained in section 2.2, reflection coefficient and reflection loss (scattering parameter s_{11}) is calculated by equation (2-12,2-13). Value of 10 and 20 dB for s-parameter (R_L) represent that 90% and 99% EM waves are absorbed by the absorbers respectively. From the figure 39, different percentage of $\text{Ni}_{0.5}\text{Zn}_{0.5}\text{Fe}_2\text{O}_4$ ferrite magnetic nanoparticles composite's (90%,10%,0.10%) scattering parameter is plotted against the frequency, this figure gives lot of information such as operating frequency, bandwidth etc. Term

bandwidth represent that at -10dB lets cut the graph, we have gap between the frequency 12.5GHz to 13GHz for 90% composite, eventually gap between the frequency 16.2GHz to 17GHz for 10% composite, 17.2GHz to 18GHz for 0.10% composite. These gaps are known as bandwidth, accordingly 10% and 0.1% gives higher bandwidth. Alternatively, operating frequency is range having higher scattering (or reflection). From the above figure, 90% composite have higher scattering upto -32dB then other. So, as per our requirements we can select the 90% or 10% or 0.10% composite. These are percentage are just an example, we have 0-100% $\text{Ni}_{0.5}\text{Zn}_{0.5}\text{Fe}_2\text{O}_4$ ferrite magnetic nanoparticles composite, analyses and select according to our requirement.

CHAPTER 7 BIBLIOGRAPHY

1. B. Dai, Y. Ren, G. Wang, Y. Ma, P. Zhu, S. Li, Microstructure and dielectric properties of biocarbon nanofiber composites, *Nanoscale research letters*, **8**(1), 293 (2013)
2. S.-T. Liu, X.-G. Chen, A.-B. Zhang, K.-K. Yan, Y. Ye, Electromagnetic Performance of Rice Husk Ash, *BioResources*, **9**(2), 2328-2340 (2014)
3. K.J. Vinoy, Radar Absorbing Materials: From Theory to Design And Characterization, *Boston: Kluwer Academic Publishers*, (1996)
4. H. Lin, H. Zhu, H. Guo, L. Yu, Investigation of the microwave-absorbing properties of Fe-filled carbon nanotubes, *Materials Letters*, **61**(16), 3547-3550 (2007)
5. X.-G. Sun, M. Gao, C. Li, Y. Wu, Microwave Absorption Characteristics of Carbon Nanotubes, (2011)
6. A. Drmota, J. Koselj, M. Drofenik, A. Žnidaršič, Electromagnetic wave absorption of polymeric nanocomposites based on ferrite with a spinel and hexagonal crystal structure, *Journal of Magnetism and Magnetic Materials*, **324**(6), 1225-1229 (2012)
7. X.-G. Chen, Y. Ye, J.-P. Cheng, Recent progress in electromagnetic wave absorbers, *Journal of Inorganic Materials*, **5**, 001 (2011)
8. K.-Y. Park, S.-E. Lee, C.-G. Kim, J.-H. Han, Fabrication and electromagnetic characteristics of electromagnetic wave absorbing sandwich structures, *Composites science and technology*, **66**(3), 576-584 (2006)
9. X. Gui, W. Ye, J. Wei, K. Wang, R. Lv, H. Zhu, F. Kang, J. Gu, D. Wu, Optimization of electromagnetic matching of Fe-filled carbon nanotubes/ferrite composites for microwave absorption, *Journal of Physics D: Applied Physics*, **42**(7), 075002 (2009)
10. X. Zhang, X. Dong, H. Huang, B. Lv, J. Lei, C. Choi, Microstructure and microwave absorption properties of carbon-coated iron nanocapsules, *Journal of Physics D: Applied Physics*, **40**(17), 5383 (2007)
11. M.-S. Cao, W.-L. Song, Z.-L. Hou, B. Wen, J. Yuan, The effects of temperature and frequency on the dielectric properties, electromagnetic interference shielding and microwave-absorption of short carbon fiber/silica composites, *Carbon*, **48**(3), 788-796 (2010)
12. W.D. Callister, Material Science and Engineering: An Introduction **Vol. 6.**(New York: John Wiley and Sons, Inc), (2000)
13. J.B. Shaffer, A. Saxena, S. D. Antolovich, T. H. S. Jr, and S. B. Warner, The Science and Design of Engineering Materials, second ed, *McGraw Hill*. 826, (1999)
14. T.B. Astrom, Manufacturing of Polymer Composites, *CRC Press*, **469**, (1997)
15. D.D.L. Chung, Carbon Fiber Composites, *Boston: Carbon Fiber Composites*, **211**, (1994)
16. S.S.S.a.J.M. Kushwaha, Preparation and characterization of magnesium ion conducting glass-polymer composites films, *Current Science* **88**(7):1159, (2005)
17. J.N.a.M.A.Z. Baucom, Low-velocity impact damage/progression in woven E-glass composite systems, *Composites, Part A: Applied Science and Manufacturing* **36A**(5):658, (2005)
18. R. Burkel, S. Deutschbein, R. Mauch, K. -h. Sossenheimer, and A. Weber, Polymer-coated composite smooth optical films for display devices for electronic components, *Schott Glas, Germany*, **p.39**, (2000)
19. K.a.S.Y. Imashita, Water-resistant glass-organic polymer composites and their manufacture *Japan*. p. 6, (1994)
20. T.a.K.Y. Osawa, Electrically conductive glass-polymer composites, *Japan*. p. 4, (1989)
21. Y. Ren, K. Yang, J. Huang, B. Zhang, and Z. Yao, Application of degradation-controllable polymer/metal composite material in medicinal implant, *Institute of Metal Research, Chinese Academy of Sciences, Peop. Rep. China*, **p. 7**, (2007)
22. E.-S. Lim, J.-C. Lee, J. -J. Kim, E.-T. Park, Y. -K. Chung, and H. -Y. Lee, Dielectric characteristics of polymer-ceramic-metal composites for the application of embedded passive devices, *Integrated Ferroelectrics* **74**:53, (2005)
23. B.C. Lavu, M. P. Schoen, and A. Mahajan, Adaptive intelligent control of ionic polymer-metal composites, *Smart Materials and Structures*, **14**(4):466, (2005)

24. M.a.K.J.K. Shahinpoor, Ionic polymer-metal composites: IV. Industrial and medical applications, *Smart Materials and Structures*, **14(1):197**, (2005)
25. J.C. Apesteguy, A. Damiani, D. DiGiovanni, S.E. Jacobo, Microwave-absorbing characteristics of epoxy resin composites containing nanoparticles of NiZn- and NiCuZn-ferrites, *Physica B: Condensed Matter*, **404(18)**, 2713-2716 (2009)
26. X. Jin, Q. Wang, W.Q. Khan, Y.Q. Li, Z.H. Tang, FeSiAl/(Ni_{0.5}Zn_{0.5})Fe₂O₄ magnetic sheet composite with tunable electromagnetic properties for enhancing magnetic field coupling efficiency, *Journal of Alloys and Compounds*, **729(Supplement C)**, 277-284 (2017)
27. B. Bammannavar, L. Naik, Electrical properties and magnetoelectric effect in (x) Ni_{0.5}Zn_{0.5}Fe₂O₄+ (1-x) BPZT composites, *Smart Materials and Structures*, **18(8)**, 085013 (2009)
28. L.A. Ramajo, A.A. Cristóbal, P.M. Botta, J.M. Porto López, M.M. Reboredo, M.S. Castro, Dielectric and magnetic response of Fe₃O₄/epoxy composites, *Composites Part A: Applied Science and Manufacturing*, **40(4)**, 388-393 (2009)
29. D. Zilli, C. Chilotte, M.M. Escobar, V. Bekeris, G.R. Rubiolo, A.L. Cukierman, S. Goyanes, Magnetic properties of multi-walled carbon nanotube-epoxy composites, *Polymer*, **46(16)**, 6090-6095 (2005)
30. N. Jebbor, S. Bri, Effective permittivity of periodic composite materials: Numerical modeling by the finite element method, *Journal of Electrostatics*, **70(4)**, 393-399 (2012)
31. D. Kechrakos, K.N. Trohidou, Competition between dipolar and exchange interparticle interactions in magnetic nanoparticle films, *Journal of Magnetism and Magnetic Materials*, **262(1)**, 107-110 (2003)
32. D. Kechrakos, K.N. Trohidou, Magnetic properties of dipolar interacting single-domain particles, *Physical Review B*, **58(18)**, 12169-12177 (1998)
33. M. Matsumoto, Y. Miyata, Thin electromagnetic wave absorber for quasi-microwave band containing aligned thin magnetic metal particles, *IEEE transactions on magnetics*, **33(6)**, 4459-4464 (1997)
34. X.e.a. Zhang, High Frequency Properties of Polymer Composites Consisting of Aligned Fe Flakes, *Journal of Applied Physics*, **08M914-08M914-3**, (2006)
35. J. Zhang, A. Kumbhar, J. He, N.C. Das, K. Yang, J.-Q. Wang, H. Wang, K.L. Stokes, J. Fang, Simple cubic super crystals containing PbTe nanocubes and their core-shell building blocks, *Journal of the American Chemical Society*, **130(45)**, 15203-15209 (2008)
36. G.V. P. Toneguzzo, O. Archer, F. Guilet, E. Bruneton, F. Fievet Vincent, F. Fievet, CoNi and FeCoNi Fine particles prepared by polyol process: Physicochemical characterization and dynamic magnetic properties *Journal of Material Science* **35,3767-3784**, (2000)
37. K. Rohlfs, Tools of radio astronomy (Tools of radio astronomy, 4th rev. and enl. ed., by K. Rohlfs and TL Wilson. Berlin, ed., Springer, 2004)
38. C. Hu, Z. Wang, W. Li, Stealth coating technology, *Chemical Industrial Publishing, Beijing*, (2004)
39. L.J. Liu SH, Dong XL, Electromagnetic wave interference shielding and absorption materials, *Chemical Industry Press, Beijing*, (2006)
40. Y. He, R. Gong, Y. Nie, H. He, Z. Zhao, Optimization of two-layer electromagnetic wave absorbers composed of magnetic and dielectric materials in gigahertz frequency band, *Journal of applied physics*, **98(8)**, 084903 (2005)
41. Dai DS, Shi FQ, Chen YQ, C. SL, Ferromagnetics, *Science Press, Beijing*, (1976)
42. W. Ellwood, V. Legg, Study of Magnetic Losses at Low Flux Densities in 35 Permalloy Sheet, *Journal of Applied Physics*, **8(5)**, 351-358 (1937)
43. J.R. Liu, M. Itoh, K.-i. Machida, Magnetic and electromagnetic wave absorption properties of α -Fe/Z-type Ba-ferrite nanocomposites, *Applied physics letters*, **88(6)**, 062503-062503-062503 (2006)
44. W. Roshen, Ferrite core loss for power magnetic components design, *Magnetics, IEEE Transactions on*, **27(6)**, 4407-4415 (1991)
45. S.P. Morgan Jr, Effect of surface roughness on eddy current losses at microwave frequencies, *Journal of Applied Physics*, **20(4)**, 352-362 (1949)
46. K. Foster, M. Littmann, Factors affecting core losses in oriented electrical steels at moderate inductions, *Journal of applied physics*, **57(8)**, 4203-4208 (1985)
47. S. Yoshida, S. Ando, Y. Shimada, K. Suzuki, K. Nomura, K. Fukamichi, Crystal structure and microwave

- permeability of very thin Fe–Si–Al flakes produced by microforging, *Journal of applied physics*, **93**(10), 6659-6661 (2003)
48. S. Yamada, E. Otsuki, Analysis of eddy current loss in Mn–Zn ferrites for power supplies, *Journal of applied physics*, **81**(8), 4791-4793 (1997)
 49. L. HR, Introduction to dielectric physics, *Chengdu University of Technology Press, Chengdu*, (1990)
 50. J. Gentner, P. Gerthsen, N. Schmidt, R. Send, Dielectric losses in ferroelectric ceramics produced by domain - wall motion, *Journal of Applied Physics*, **49**(8), 4485-4489 (1978)
 51. J. Qiu, Y. Wang, M. Gu, Microwave absorption properties of substituted BaFe₁₂O₁₉/TiO₂ nanocomposite multilayer film, *Journal of materials science*, **42**(1), 166-169 (2007)
 52. A. Yusoff, M. Abdullah, S. Ahmad, S. Jusoh, A. Mansor, S. Hamid, Electromagnetic and absorption properties of some microwave absorbers, *Journal of Applied Physics*, **92**(2), 876-882 (2002)
 53. J. Huo, L. Wang, H. Yu, Polymeric nanocomposites for electromagnetic wave absorption, *Journal of materials science*, **44**(15), 3917-3927 (2009)
 54. Z.K. Deng LW, Jiang JJ, Feng ZQ, *Cent South Univ: Sci Technol* 39:59 (2008)
 55. Z. Guo, S. Park, H.T. Hahn, S. Wei, M. Moldovan, A.B. Karki, D.P. Young, Magnetic and electromagnetic evaluation of the magnetic nanoparticle filled polyurethane nanocomposites, *Journal of applied physics*, **101**(9), 09M511 (2007)
 56. B.J. Xue KH, Nano chemistry: the chemical construction and applications of nanosystems, *Chemical Industry Press, Beijing*, (2006)
 57. S.A. Jylha. L, Differential Equation for the Effective Permittivity of Random Mixture of Spheres, *International URSI Commission B-Electromagnetic Theory Symposium*, **Ottawa, 26-28**, (2007)
 58. F.S. KH Chew, B Ploss, HLW Chan, CL Choy, Primary and secondary pyroelectric effects of ferroelectric 0-3 composites, *Journal of Applied Physics*, **94**(2), **1134-1145** (2003)
 59. R. Hill, Elastic properties of reinforced solids: Some theoretical principles, *Journal of the Mechanics and Physics of Solids*, **11**(5), 357-372 (1963)
 60. Evaluating Electrically Insulating Epoxies, http://www.adhesives.org/docs/pdfs/electrically_insulative_epoxies.pdf?sfvrsn=0
 61. H. Lee, K. Neville, Handbook of epoxy resins, McGraw-Hill, 1967
 62. C.-H. Peng, C.-C. Hwang, J. Wan, J.-S. Tsai, S.-Y. Chen, Microwave-absorbing characteristics for the composites of thermal-plastic polyurethane (TPU)-bonded NiZn-ferrites prepared by combustion synthesis method, *Materials Science and Engineering: B*, **117**(1), 27-36 (2005)
 63. A. Thakur, P. Kumar, P. Thakur, K. Rana, A. Chevalier, J.L. Mattei, P. Queffelec, Enhancement of magnetic properties of Ni_{0.5}Zn_{0.5}Fe₂O₄ nanoparticles prepared by the co-precipitation method, *Ceramics International*, **42**(9), 10664-10670 (2016)
 64. Y. Jiang, M. Opoku, Z. Hu, M. Liu, H. Hong, J.A. Puszynski, X. Yan, Synthesis and Characterization of Spinel Ferrite Based Nanofluids, *Journal of Nanofluids*, **4**(2), 133-139 (2015)
 65. S.A. Saafan, T.M. Meaz, E.H. El-Ghazzawy, Study of DC conductivity and relative magnetic permeability of nanoparticle NiZnFe₂O₄/PPy composites, *Journal of Magnetism and Magnetic Materials*, **323**(11), 1517-1524 (2011)
 66. A.G.T. M. Jalali, R. Wuthrich,, Fabrication of Metallic Nanoparticles through Waste of Micro-EDM, *EUSPEN, San Sebastian*, (2009)
 67. J. Dormann, D. Fiorani, E. Tronc, Magnetic relaxation in fine - particle systems, *Advances in Chemical Physics*, *Volume 98*, 283-494 (2007)
 68. M.D. HW Hong, Preparation method od epoxy composite material on basis of nano silica particles, *Google Patent*, **CN 201310315641** (2013)
 69. C.L. HT Zhao, Magneto-calorific curing method for thermosetting resin adhesive, *Google Patent*, **CN 201410627698**, (2015)